Elsevier Editorial System(tm) for International Journal of Mechanical Sciences
Manuscript Draft

Manuscript Number:

Title: Path tracking and stability of a rolling controlled wheel on a horizontal plane by using the nonholonomic constraints

Article Type: Research Paper

Keywords: Rolling Wheel; Nonholonomic Constraints; Control Torque; Path Tracking; Set Point; Stability.

Corresponding Author: Dr. Manuel F. Perez-Polo, Doctor

Corresponding Author's Institution: Universidad de Alicante

First Author: Javier Gil-Chica, Dr

Order of Authors: Javier Gil-Chica, Dr; Manuel Perez-Molina, Dr; Manuel F. Perez-Polo, Doctor

Abstract: This paper studies the stabilization, tracking of a predefined trajectory and how to reach a desired set point for a wheel which is rolling on a horizontal plane without slipping. For this purpose, the wheel is controlled by small torque generated by internal servomechanisms whose dynamics can be neglected. An efficient procedure to determine the kinetic energy of the wheel is developed by introducing a set of reference systems, which in combination with the Lagrange equations with multipliers allow deriving the mathematical model of the rolling wheel. In this model, the Euler angles, the coordinates of the plane-wheel contact point and a control law of proportional + integral + derivative (PID) type provide an efficient computational procedure to track arbitrary trajectories. It is shown that the nonholonomic constraints are fulfilled with admissible reaction forces, even when the desired trajectory has cusp points. A circumference and a family of astroids are used as trajectories to verify the motion conditions derived from the energy conservation and dynamical equilibrium of the wheel along such trajectories. The results of the analytical calculations are corroborated through numerical simulations.

Cover Letter

Dear Editor,

We are submitting the manuscript entitled “Path tracking and stability of a rolling controlled wheel on a horizontal plane by using the nonholonomic constraints” to be considered for publication in International Journal of Mechanical Sciences.

Yours Sincerely,

The authors

Highlights

- New method to obtain the kinetic energy of a rolling body using rotation matrices.
- Stability analysis of a rolling wheel with and without control torques.
- Procedure to obtain stable circular trajectories with very small control torques.
- Procedure to track arbitrary trajectories with cusp points by using PID control.
- Fulfillment of the nonholonomic constraints in all analyzed motions.

Path tracking and stability of a rolling controlled wheel on a horizontal plane by using the nonholonomic constraints

Javier Gil Chica[a], Manuel Pérez Molina[b], Manuel F. Pérez Polo[c*]

Departamento de Física, Ingeniería de Sistemas y Teoría de la Señal, Universidad de Alicante, Escuela Politécnica Superior, Campus de San Vicente, 03071, Alicante, Spain. Fax 34-9-659-09750, [a]Tel: 34-9-659-09673. E-mail: gil@dfists.ua.es, [b]Tel: 34-9-659-02077. E-mail: ma_perez_m@hotmail.com [c*]Tel: 34-9-659-09673. E-mail: manolo@dfists.ua.es

Abstract

This paper studies the stabilization, tracking of a predefined trajectory and how to reach a desired set point for a wheel which is rolling on a horizontal plane without slipping. For this purpose, the wheel is controlled by small torque generated by internal servomechanisms whose dynamics can be neglected. An efficient procedure to determine the kinetic energy of the wheel is developed by introducing a set of reference systems, which in combination with the Lagrange equations with multipliers allow deriving the mathematical model of the rolling wheel. In this model, the Euler angles, the coordinates of the plane-wheel contact point and a control law of proportional + integral + derivative (PID) type provide an efficient computational procedure to track arbitrary trajectories. It is shown that the nonholonomic constraints are fulfilled with admissible reaction forces, even when the desired trajectory has cusp points. A circumference and a family of astroids are used as trajectories to verify the motion conditions derived from the energy conservation and dynamical equilibrium of the wheel along such trajectories. The results of the analytical calculations are corroborated through numerical simulations.

Keywords: Rolling Wheel, Nonholonomic Constraints, Control Torque, Path Tracking, Set Point, Stability.

[c*]Author whose correspondence should be addressed

1 Introduction

The nonholonomic mechanical problem of a wheel that rolls on a horizontal plane is emblematic in the history of rigid solid dynamics. Studies about this problem begun in the XIX century and were considered in the classical works of Chaplygin, Routh, Hamel, Appell and Korteweg, among others [1-4]. More recently, a wheel assimilated to a disk or a torus that rolls on a horizontal plane without involving control torques has been analyzed in Refs. [4-7]. On the other hand, the differential geometry approach currently offers a powerful tool in the new developments of mechanics such as nonholonomic systems [8-10] and the controlled motion of wheeled mobile robots, which have become the subject of numerous research studies [11-14] (see also references cited therein).

The stability of a wheeled vehicle is closely related to the kinematics and dynamics of a wheel, including friction and deformation [15,16] as well as effects of non ideal contact between the surfaces of rolling bodies as it can be found in Ref [4, Chapter IV] and in Refs [17-19]. Currently, non-ideal contact problems of wheels rolling on surfaces of several materials can be found in Refs [20-21] and in the references therein contained. On the other hand, the control and guidance of a rolling disk on a horizontal plane has been analyzed assuming that the motion of the disk is controlled by torques generated by internal servomechanisms, slender rods and rotors [22-24]. A prototype is the so called gyrover, which in essence is a single-wheel robot with a gyroscopic stabilization mechanism and an adequate pedaling torque [25].

In this work we derive the nonholonomic constraints of a rolling wheel on a horizontal plane through geometrical considerations and then we deduce the kinetic energy by using an adequate definition of a set of reference systems. Once the kinetic energy and the nonholonomic constraints have been obtained, the mathematical model of the wheel is deduced by using the Euler angles and the coordinates of the contact point between the wheel and the supporting plane. By using such mathematical model in combination with an adequate control law, we demonstrate the possibility of tracking of a predefined trajectory and reaching an arbitrary desired set point for the wheel. In a previous study [26], a rolling disk that can reach a predetermined set point (regardless the followed trajectory) has been investigated by using the Newton-Euler equations.

However, the current paper aims to track of a predetermined trajectory for a rolling wheel that can be assimilated to a torus, and the nonholonomic constraints are different than the ones of Ref. [26]. Other examples of related rolling disks can be found in Refs [17], [22-24] and [27].

To carry out our study, we first analyze the limit values of the rotation velocity to obtain a stable rolling wheel without control torques. Assuming that a friction rolling torque is present, the motion of the wheel is also analyzed, showing that the energy conservation principle is verified. Since the wheel without control torques is very unstable, a stabilizing torque around the leaning angle is added, showing that in this case the angular velocity of the wheel can be drastically reduced.

On the basis of the nonholonomic conditions it is shown that the wheel can be driven along a circumference. In this case, it is verified that the analytical expressions for the radius of the circle and the coordinates of the trajectory center are in agreement with numerical simulations. Besides, the conditions of dynamical equilibrium between the centrifugal force and the lateral reaction force at the contact point wheel-plane are fulfilled with a small stabilization torque [1-4], [27].

The tracking of a prescribed trajectory is obtained by eliminating the Euler angles between the differential equations that define the coordinates of the contact point wheel-plane and the equations that arise from assuming fictitious forces applied at the mass center of the wheel. In the resulting equations, a control law of PID type is designed so that the error between the actual and the desired trajectory tends to zero. The stability conditions for the integral action of the PID controller are analyzed from the Routh's criterion of stability [28]. This procedure has the advantage of obtaining small torques even when the control is applied abruptly, and thus the dynamics of the internal servomechanisms responsible for the control torques can be neglected. In addition it is shown that it is possible to track trajectories with cusp points and to jump to a prescribed set point from an arbitrary point of the tracked trajectory.

2 Nonholonomic constraints and mathematical model of the wheel

In this section, the nonholonomic constraints and the mathematical model of the wheel are analyzed. Let us consider a wheel modeled by a torus assuming that its mass is uniformly distributed along its surface and that its geometrical center coincides with the center of mass of the torus. In addition, the masses of the servomechanisms which will generate the control torques are assumed to be located in the mass center of the torus. As notation criterion, b shall denote the curvature radius of the torus meridian (i.e. the outer radius of the torus) and $a + b$ shall denote the radius of the equatorial circle of the torus. On the other hand, p, q and r are the precession, leaning and spin angles respectively, which define the orientation of the torus with respect to a fixed reference frame $OXYZ$. Thus $(\dot{p}, \dot{q}, \dot{r})$ are the corresponding angular velocities of the angles (p,q,r) defined with respect to the moving reference system $G\xi\eta\zeta$ bounded to the torus, as shown in Fig 1 a). The magnitudes (p,q,r) are the classical Euler angles (also denoted by $\psi \equiv p$, $\theta \equiv q$ and $\varphi \equiv r$ [1-4], [6], [27]), for which the considered notation in this paper aims to ease the discussion of the mathematical model. The magnitudes λ and μ are the reaction forces located in the OXY plane, which will be interpreted as Lagrange multipliers.

2.1 Nonholonomic constraints

Our first purpose is to determine the nonholonomic constraints of the torus when it is rolling on a horizontal plane, assuming that C is the only contact point between the torus and the supporting plane. To do this aim, from Fig 1 b) it is deduced that the two curvature radii due to the rolling movement around point C are a and $CM = PG = b + a\sin q$. Assuming that dS_1 and dS_2 are infinitesimal displacements of the contact point C, we can write that:

$$dS_1 = a\,dq \;\; ; \;\; dS_2 = (b + a\sin q)\,dr \tag{1}$$

where the curvature radius a is associated to the rotation defined by the leaning angle q and the curvature radius $b + a\sin q$ is due to the infinitesimal change of the spin angle r.

The values of dS_1 and dS_2 are plotted in Fig 1 c). By projecting dS_1 and dS_2 on the OX and OY axes it follows that:

$$\left.\begin{aligned} dx &= dS_1 \sin p - dS_2 \cos p \\ dy &= -dS_1 \cos p - dS_2 \sin p \end{aligned}\right\} \tag{2}$$

On the other hand, substituting Eqs (1) into Eqs (2) and dividing the resulting equation by *dt*, Eqs (2) can be rewritten as:

$$\left.\begin{aligned} \dot{x} &= -\dot{r}\left(b + a\sin q\right)\cos p + a\dot{q}\sin p \\ \dot{y} &= -\dot{r}\left(b + a\sin q\right)\sin p - a\dot{q}\cos p \end{aligned}\right\} \tag{3}$$

where the upper dot indicates derivative with respect to the time. Eqs (3) are the nonholonomic conditions assuming pure rolling of the torus on the horizontal plane. It should be noticed that the coordinates *(x,y)* of point *C* define the successive contact points between the torus and the supporting plane, which form a trajectory that is followed with a translation velocity $\left(\dot{x}, \dot{y}\right)$. Such translation velocity is the one that an observer could perceive if he/she were unable of noticing the combined rotation motions of the wheel. However, the point of the torus in contact with the horizontal plane has zero relative velocity with respect to the *OXYZ* reference system. In some references [1-3], [6] equivalent nonholonomic conditions are obtained assuming that the velocity of the contact point between the body and the plane is zero.

Figure 1

2.2 Mathematical model of the wheel rolling on a horizontal plane

The following step in our analysis is to derive the mathematical model of the system taking into account the nonholonomic constraints defined by Eqs (3). This model is obtained by using the Euler-Lagrange equations, so it is necessary to obtain the kinetic and potential energies referred to the inertial frame *OXYZ* [1-4]. In the model of the wheel motion it is necessary to take into account the nonholonomic constraints

given by Eqs (3). For this purpose, the following vectors and reference systems are introduced in Fig 2 a):

i) The inertial reference frame is denoted by *'o'* and $\vec{R}(t)$ is the position vector of the contact point *C* with respect to *'o'*.

ii) The reference system *'i'* has their axes parallel to the ones of system *'o'* and its origin is at the contact point *C*. On the other hand, $\vec{r}_i(t)$ is the position vector of the mass center *G* of the wheel with respect to *'i'*.

iii) The reference system *'s'* has its origin at the mass center G of the wheel and its axes are parallel to the ones of system *'o'*. In the reference system *'s'*, $\vec{r}_s(t)$ shall denote the position vector of an arbitrary point *P* of the torus surface.

iv) Finally, we introduce another reference system *'p_b'* with origin at *G* and bounded to the torus. In this reference system, $\vec{r}_p(t)$ will be the position vector of a generic point of the torus surface, which is related to $\vec{r}_s(t)$ by means of rotation matrix $\bar{R}_{pqr}$ (see Appendix 1) as $\vec{r}_s(t) = \bar{R}_{pqr}\vec{r}_p(t)$.

Taking into account the previous definitions and Fig 2a), it is deduced that:

$$\vec{r}_O(t) = \vec{R}(t) + \vec{r}_i(t) + \vec{r}_s(t) = \vec{R}(t) + \vec{r}_i(t) + \bar{R}_{pqr}\vec{r}_p(t) \tag{4}$$

Since $\vec{r}_p(t)$ remains unaltered in the reference system *'p_b'* (bounded to the wheel), it holds that the derivative of $\vec{r}_p(t)$ with respect to the time is zero, so differentiating in both sides of Eq (4) with respect to the time it follows that:

$$\dot{\vec{r}}_O(t) = \dot{\vec{R}}(t) + \dot{\vec{r}}_i(t) + \dot{\bar{R}}_{pqr}\vec{r}_p(t) \tag{5}$$

where the components of $\dot{\vec{R}}(t), \dot{\vec{r}}_i(t)$ and $\vec{r}_p$ in the inertial frame *OXYZ* are given by:

$$\dot{\vec{R}} = \begin{bmatrix} \dot{x} \\ \dot{y} \\ 0 \end{bmatrix} ; \dot{\vec{r}}_i = \begin{bmatrix} -b\cos q\cos p \\ -b\cos q\sin p \\ 0 \end{bmatrix} \dot{p} + \begin{bmatrix} b\sin q\sin p \\ -b\sin q\cos p \\ 0 \end{bmatrix} \dot{q}$$
$$\vec{r}_p = \begin{bmatrix} (b + a\cos m)\cos n \\ (b + a\cos m)\sin n \\ a\sin m \end{bmatrix} \tag{6}$$

whereas the elements of matrices $\bar{R}_{pqr}$ and $\dot{\bar{R}}_{pqr}$ are given in Appendix 1. On the other hand, the surface of the wheel is $4\pi^2 ab$ and thus its mass surface density is $\sigma = M/4\pi^2 ab$, being *M* the total mass of the torus. Fig 2 b) shows the basic geometry of the torus as a function of the angles *m* and *n*, from which it can be deduced that the surface element *dS* and the element of mass $d\upsilon$ of the wheel are given by:

$$dS = a(b + a\cos m)\,dmdn \; ; \; d\upsilon = \sigma a(b + a\cos m)\,dmdn \tag{7}$$

Taking into account Eqs (5) and (7), the kinetic energy of an element of mass with respect to the reference frame OXYZ can be written as:

$$dT = \frac{1}{2}\sigma \dot{\vec{r}}_O^{\,2} a(b + a\cos m)\,dmdn \tag{8}$$

Figure 2

The total kinetic energy is obtained by integrating Eq (8) with respect to *m* and *n*. Such integration can be carried out through symbolic computation by introducing the following nomenclature:

$$\dot{\vec{r}}_O^{\,2} = \left[\dot{\bar{R}}(t) + \dot{\vec{r}}_i(t) + \dot{R}_{pqr}\vec{r}_p(t)\right]^T \left[\dot{\bar{R}}(t) + \dot{\vec{r}}_i(t) + \dot{R}_{pqr}\vec{r}_p(t)\right] \tag{9}$$

The integration is first carried out with respect to angle *n* and afterwards with respect to angle *m*. By doing so, for each term of Eq (8) it is necessary to calculate the integral given by:

$$\frac{1}{2}\int_0^{2\pi} dm \int_0^{2\pi} T_i \sigma a\left(b + a\cos m\right) dn \tag{10}$$

On the other hand, the kinetic energy of the servomechanism mass M_1 -whose mass center coincides with the one of the wheel-, can be calculated taking into account Eqs (5) and (6), which leads to (see Fig 2 a):

$$T_{M_1} = \frac{1}{2} M_1 \left[\dot{\vec{R}}(t) + \dot{\vec{r}}_i(t)\right]^T \left[\dot{\vec{R}}(t) + \dot{\vec{r}}_i(t)\right] \tag{11}$$

The result of adding the integral in Eq (10) to the kinetic energy of Eq (11) is given by:

$$\begin{gathered} T = \frac{1}{2} M_T \left(\dot{x}^2 + \dot{y}^2\right) + \\ M_T b\left(\dot{x}\dot{q}\sin p \sin q - \dot{y}\dot{p}\sin p\cos q\right) - M_T b\left(\dot{x}\dot{p}\cos p\cos q + \dot{y}\dot{q}\cos p\sin q\right) \\ + c\dot{p}^2\cos^2 q + d\dot{p}^2 + e\dot{q}^2 + f\dot{r}^2 + \bar{g}\dot{p}\dot{r}\cos q \end{gathered} \tag{12}$$

where:

$$\begin{gathered} M_T = M + M_1 \;;\; c = \frac{1}{2}Mb^2 + \frac{1}{8}M\left(a^2 + b^2\right) + \frac{1}{2}M_1 b^2 \;;\; d = \frac{1}{8}M\left(5a^2 + 2b^2\right) \\ e = \frac{1}{2}Mb^2 + \frac{1}{8}M\left(5a^2 + 2b^2\right) + \frac{1}{2}M_1 b^2 \;;\; f = \frac{1}{4}M\left(3a^2 + 2b^2\right) \;;\; \bar{g} = \frac{1}{2}M\left(3a^2 + 2b^2\right) \end{gathered} \tag{13}$$

Taking into account that the potential energy of the wheel is:

$$V = M_T g\left(a + b\sin q\right) \tag{14}$$

The Lagrangian of the system can be written as follows:

$$\begin{gathered} L = T - V = \frac{1}{2} M_T \left(\dot{x}^2 + \dot{y}^2\right) + M_T b\left(\dot{x}\dot{q}\sin p\sin q - \dot{y}\dot{p}\sin p\cos q\right) - \\ M_T b\left(\dot{x}\dot{p}\cos p\cos q + \dot{y}\dot{q}\cos p\sin q\right) + c\dot{p}^2\cos^2 q + d\dot{p}^2 + e\dot{q}^2 + f\dot{r}^2 + \bar{g}\dot{p}\dot{r}\cos q - \\ - M_T g\left(a + b\sin q\right)\Big) \end{gathered} \tag{15}$$

An interesting aspect of Eq (15) is related to the fact that the coordinates *(x,y)* of the successive contact points between the wheel and the supporting plane appear as generalized coordinates. This fact can be used to investigate which control torques must be applied so that the wheel follows a predetermined trajectory on the OXY plane to finally reach a predefined set point.

It should be remarked that the substitution of the variables *(x,y)* of the nonholonomic constraints (Eqs (3)) into Eq(15) allows to obtain a Lagrangian that only involves the Euler angles. However, such Lagrangian does not verify the Lagrange equations, as has been proved in Ref [2] (pag 382) and Ref [27] (chapter 22). This is because the system is nonholonomic and thus the Lagrange equations cannot be applied directly, but it is necessary to introduce the Lagrange multipliers [1-4], [26], [27], which are identified with the reaction forces λ and μ that are indicated in Fig 1 a) and Fig 2 a).

It should also be noticed that the coordinates *(x,y)* of the wheel-plane contact point and the Euler angles *(p,q,r)* constitute five unknown generalized coordinates, and additionally we have two unknown reaction forces *(λ, μ).* From the Lagrangian given by Eq (15) it is possible to deduce five equations associated to each of the generalized coordinates, and considering jointly the nonholonomic constraints given by Eqs (3) we obtain a system of seven equations with seven unknowns. In addition, to track a path for the wheel it is necessary to introduce a precession control torque $M_p(t)$, a leaning control torque $M_q(t)$ and a pedaling control torque $M_q(t)$. In this case, the corresponding control equations must be added so that we have a well posed problem, as it will be investigated in the next section. The Lagrange equations allow to deduce the following equations of motion:

$$M_T\ddot{x} + M_T b\left[-\ddot{p}\cos p\cos q + \ddot{q}\sin p\sin q + \left(\dot{p}^2+\dot{q}^2\right)\sin p\cos q + 2\dot{p}\dot{q}\cos p\sin q\right] = \lambda\cos p - \mu\sin p \tag{16}$$

$$M_T\ddot{y} - M_T b\left[\ddot{p}\sin p\cos q + \ddot{q}\cos p\sin q + \left(\dot{p}^2+\dot{q}^2\right)\cos p\cos q - 2\dot{p}\dot{q}\sin p\sin q\right] = \lambda\sin p + \mu\cos p \tag{17}$$

$$-M_T b\ddot{x}\cos p\cos q - M_T b\ddot{y}\sin p\cos q + 2c\ddot{p}\cos^2 q - 4c\dot{p}\dot{q}\cos p\cos q + 2d\ddot{p} + \bar{g}\dot{r}\cos q - \bar{g}\dot{r}\dot{q}\sin q = Q_p \tag{18}$$

$$M_T b\ddot{x}\sin p\sin q - M_T b\ddot{y}\cos p\sin q + 2c\ddot{q} + 2c\dot{p}^2\cos p\sin q + \bar{g}\dot{p}\dot{r}\sin q + Mgb\cos q = Q_q \tag{19}$$

$$2f\ddot{r} + \ddot{p}\bar{g}\cos p - \dot{p}\dot{q}\bar{g}\sin q = Q_r \tag{20}$$

where Q_p, Q_q and Q_r are the generalized torques [1-4], [26], [27]. These torques can be obtained by considering a cross section of the wheel as it appears in Fig 1 b). First, it should be noted that the force μ does not contribute to generate the angular velocity $\dot{p}$, so only the force λ (at right angle with the wheel section plotted in Fig 1 b)) generates the generalized torque given by:

$$Q_p = \lambda CQ = \lambda b\cos q \tag{21}$$

Since the angle velocity $\dot{q}$ is parallel to the OXY plane (see Fig 2 a) and it forms a right angle with the cross section of Fig 1 b), it is deduced that:

$$Q_q = \mu GQ = \mu\left(a + b\sin q\right) \tag{22}$$

On the other hand, the reaction force μ cannot give rise to a rotation of the wheel around the mass center G, so only the reaction force λ can generate the torque Q_r and thus it is deduced that:

$$Q_r = \lambda PG = \lambda\left(b + a\sin q\right) \tag{23}$$

It should be noticed that the reference systems that are considered to determine the kinetic energy (which are plotted in Fig 2 a)) can also be used to derive the nonholonomic constraints given by Eqs (3). To corroborate this assertion we note that point *O* of the torus surface (see Fig 2 a)) is an arbitrary point, so Eq (5) can be applied to the contact point *C* between the wheel and the plane. Assuming that the wheel rolls without slipping, point C has null velocity with respect to the supporting surface, so Eq (5) allows determining the nonholonomic conditions as follows:

$$\vec{0} = \dot{\vec{R}}(t) + \dot{\vec{r}}_i(t) + \dot{R}_{pqr}\vec{r}_p(t) \tag{24}$$

Taking into account the equations of the rotation matrix and its derivate with respect to the time indicated in Appendix 1, the symbolic computation of Eq (24) gives the same results as in Eqs (3). It is interesting to remark that Eq (24) is general and can be applied to obtain the nonholonomic constraints of a wheel that rolls on an arbitrary surface of class C^n with n ≥ 2.

3 Stability of the wheel motion and nonholonomic constraints

Once the mathematical model of the wheel has been obtained from Eqs (16-23) of the previous section, we are going to develop a procedure to obtain an efficient computational program for integrating these equations. Since the model of the wheel has been deduced from the hypothesis of rolling without slipping (which is equivalent to say that the nonholonomic constraints of Eqs (3) are fulfilled), it is very important to corroborate that Eqs (3) are verified. For this purpose, different trajectories will be investigated from a set of initial conditions, and a procedure to elucidate if the nonholonomic conditions are verified will be outlined. In addition, since the wheel is highly unstable, a stabilization torque around the leaning angle q must be introduced to warrant the motion stability. Differentiating Eqs (3) of the nonholonomic constraints with respect to the time it is obtained that:

$$\begin{aligned}\ddot{x} = &-\ddot{r}\left(b + a\sin q\right)\cos p - \dot{r}\left(-a\dot{p}\sin p\sin q + a\dot{q}\cos p\cos q - b\dot{p}\sin p\right)\\ &+ a\ddot{q}\sin p + a\dot{p}\dot{q}\cos p\end{aligned} \tag{25}$$

$$\begin{aligned}\ddot{y} = &-\ddot{r}\left(b + a\sin q\right)\sin p - \dot{r}\left(a\dot{p}\cos p\sin q + a\dot{q}\sin p\cos q + b\dot{p}\sin p\right)\\ &- a\ddot{q}\cos p + a\dot{p}\dot{q}\sin p\end{aligned} \tag{26}$$

Substituting Eqs (25) and (26) into Eqs (16) and (17) respectively, we obtain equations of the form:

$$\left.\begin{aligned} f_{x2} + f_{x1} &= \lambda\cos p - \mu\sin p\\ f_{y2} + f_{y1} &= \lambda\sin p + \mu\cos p\end{aligned}\right\} \tag{27}$$

where f_{x2} and f_{y2} are the terms that only contain second-order derivatives of the Euler angles (i.e. $\ddot{p},\ddot{q},\ddot{r}$) whereas f_{x1} and f_{y1} are the terms that only contain first-order derivatives of the Euler angles (i.e. $\dot{p},\dot{q},\dot{r}$), so it follows that:

$$\left.\begin{aligned} f_{x2} &= -M_T b\cos p\cos q\ddot{p} + M_T\left(a+b\sin q\right)\sin p\ddot{q} - M_T\left(b+q\sin q\right)\cos p\ddot{r} \\ f_{y2} &= -M_T b\sin p\cos q\ddot{p} + M_T\left(a+b\sin q\right)\cos p\ddot{q} - M_T\left(b+q\sin q\right)\sin p\ddot{r} \end{aligned}\right\} \tag{28}$$

$$\left.\begin{aligned} f_{x1} &= -M_T\dot{r}\left(-a\dot{p}\sin p\sin q + a\dot{q}\cos p\cos q - b\dot{p}\sin p\right) + M_T a\dot{p}\dot{q}\cos p + \\ &\quad M_T b\left[\left(\dot{p}^2+\dot{q}^2\right)\sin p\cos q + 2\dot{p}\dot{q}\cos p\sin q\right] \\ f_{y1} &= -M_T\dot{r}\left(-a\dot{p}\cos p\sin q + a\dot{q}\sin p\cos q + b\dot{p}\cos p\right) + M_T a\dot{p}\dot{q}\sin p + \\ &\quad M_T b\left[\left(\dot{p}^2+\dot{q}^2\right)\cos p\cos q - 2\dot{p}\dot{q}\sin p\sin q\right] \end{aligned}\right\} \tag{29}$$

According to Eqs (27), the reaction forces λ and μ can be written as:

$$\left.\begin{aligned} \lambda &= \left(f_{x2}\cos p + f_{y2}\sin p\right) + \left(f_{x1}\cos p + f_{y1}\sin p\right) \\ \mu &= \left(-f_{x2}\sin p + f_{y2}\cos p\right) + \left(-f_{x1}\sin p + f_{y1}\cos p\right) \end{aligned}\right\} \tag{30}$$

Substituting Eqs (25), (26), (28)-(30) into Eqs (18)-(20) and taking into account Eqs (21)-(23) (generalized torques), the equations associated to Euler angles can be expressed as:

$$\left.\begin{aligned} M_{11}\ddot{p} + M_{12}\ddot{q} + M_{13}\ddot{r} &= f_1 \\ M_{21}\ddot{p} + M_{22}\ddot{q} + M_{23}\ddot{r} &= f_2 \\ M_{31}\ddot{p} + M_{32}\ddot{q} + M_{33}\ddot{r} &= f_3 \end{aligned}\right\};\ \mathbf{M} = \begin{bmatrix} M_{11} & M_{12} & M_{13} \\ M_{21} & M_{22} & M_{23} \\ M_{31} & M_{32} & M_{33} \end{bmatrix} \tag{31}$$

where the coefficients M_{ij} only depend on the Euler angles $\left(p,q,r\right)$ whereas the functions f_i depend both on the Euler angles $\left(p,q,r\right)$ and its derivatives with respect to time, i.e.:

$$\left.\begin{aligned} M_{ij}\left(t\right) &= M_{ij}\left(p,q,r\right)\ ;\ i,j=1,2,3 \\ f_i\left(t\right) &= f_i\left(p,q,r,\dot{p},\dot{q},\dot{r}\right)\ ;\ i=1,2,3 \end{aligned}\right\} \tag{32}$$

Specifically, the coefficients M_{ij} which are not null and the coefficients f_i *(i = 1,2,3)* are given by:

$$\left.\begin{aligned} M_{11} &= 2c\cos^2 q + 2d + M_T b^2 \cos^2 q \\ M_{13} &= 2M_T b\cos q\left(b + a\sin q\right) + \bar{g}\cos q \\ M_{22} &= M_T ab\sin q + 2c + M_T\left(a + b\sin q\right)^2 \\ M_{31} &= \bar{g}\cos q + M_T b\left(b + a\sin q\right)\cos q \\ M_{33} &= 2f + M_T\left(b + a\sin q\right)^2 \end{aligned}\right\} \tag{33}$$

$$\left.\begin{aligned} f_1 &= -M_T b\sin p\cos q\dot{r}\left(a\dot{p}\cos p\sin q + a\dot{q}\sin p\cos q + b\dot{p}\cos p\right) \\ &\quad + M_T ab\cos q\dot{p}\dot{q} \\ &\quad - M_T b\cos p\cos q\dot{r}\left(-a\dot{p}\sin p\sin q + a\dot{q}\cos p\cos q - b\dot{p}\sin p\right) \\ &\quad + 4c\dot{p}\dot{q}\cos q\sin q + \bar{g}\dot{r}\dot{q}\sin q + b\left(f_{x1}\cos p + f_{y1}\sin p\right)\cos q \\ f_2 &= -M_T b\sin p\sin q\dot{r}\left(-a\dot{p}\sin p\sin q + a\dot{q}\cos p\cos q - b\dot{p}\sin p\right) \\ &\quad + M_T b\cos p\sin q\dot{r}\left(a\dot{p}\cos p\sin q + a\dot{q}\sin p\cos q + b\dot{p}\cos p\right) \\ &\quad - cc\dot{p}^2\cos q\sin q - \bar{g}\dot{p}\dot{r}\sin q - M_T gb\cos q \\ &\quad + \left(-f_{x1}\sin p + f_{y1}\cos p\right)\left(a + b\sin q\right) \\ f_3 &= \bar{g}\dot{p}\dot{q}\sin q + \left(f_{x1}\cos p + f_{y1}\sin p\right)\left(b + a\sin q\right) \end{aligned}\right\} \tag{34}$$

It is interesting to remark that the coefficients M_{ii} *(i = 1,2,3)* in Eqs (33) are non zero regardless the values of the Euler angles, and therefore the matrix **M** given in Eq (31) has always inverse, i.e. we have a well posed problem. Next, from Eqs (31), (33) and (34) the stability of the wheel will be analyzed. For this purpose, Eq (31) can be rewritten taking into account the inverse of matrix **M** as follows:

$$\left.\begin{aligned} \frac{d^2 p(t)}{dt^2} &= \frac{M_{22}(t)}{\Delta(t)}\left[M_{33}(t)\,f_1(t) - M_{13}(t)\,f_3(t)\right] \\ \frac{d^2 q(t)}{dt^2} &= \frac{f_2(t)}{M_{22}(t)} \;\; ; \;\; \Delta(t) = M_{22}(t)\left[M_{11}(t)M_{33}(t) - M_{13}(t)M_{31}(t)\right] \\ \frac{d^2 r(t)}{dt^2} &= \frac{M_{22}(t)}{\Delta(t)}\left[-M_{31}(t)\,f_1(t) + M_{11}(t)\,f_3(t)\right] \end{aligned}\right\} \tag{35}$$

From a physical viewpoint, a stable rolling motion of the wheel will be achieved if the angular velocity is sufficiently high to maintain the wheel in vertical position, i.e. with a leaning angle of π/2. This case can be investigated through the linearization of Eqs (35) and assuming a small disturbance for the leaning angle around its equilibrium value of π/2, for which the deviation variable *α(t)* is defined as:

$$q(t)=\frac{\pi}{2}-\alpha(t)\ \ ;\ \ \alpha(t)\ll 0 \Rightarrow \left.\begin{cases}\cos q(t)=\sin\alpha(t)\approx\alpha(t)\\ \sin q(t)\approx 1\\ \dot{q}(t)=-\dot{\alpha}(t)\ \ ;\ \ \ddot{q}(t)=-\ddot{\alpha}(t)\end{cases}\right\} \tag{36}$$

From Eqs (36), Eqs (33) can be approximated as follows:

$$\left.\begin{array}{c} M_{11}\approx 2d\ \ ;\ \ M_{13}\approx\left[\bar{g}+2M_T b(a+b)\right]\alpha \\ M_{22}\approx 2c+M_T ab+M_T(a+b)^2\ \ ;\ \ M_{31}\approx\left[\bar{g}+M_T b(a+b)\right]\alpha \\ M_{33}\approx 2f+M_T(b+a)^2 \end{array}\right\} \tag{37}$$

Taking into account Eqs (29) and (36), and assuming a motion that is almost perpendicular to the supporting plane, it is possible to take $\dot{p}\alpha\approx 0$ when the precession velocity is very small (i.e. when the trajectory of the wheel approaches to a straight line). Consequently, from Eqs (34) it is deduced that:

$$f_1\approx\bar{g}\dot{q}\dot{r}-2M_T ab\dot{p}\dot{\alpha}\alpha-2M_T b^2\dot{p}\dot{\alpha}\alpha\approx\bar{g}\dot{q}\dot{r} \tag{38}$$

On the other hand, assuming that $\dot{\alpha}\alpha\approx 0$ and $\dot{p}\dot{\alpha}\approx 0$, Eqs (29) and (34) allow to approximate the values of the functions f_2 and f_3 as:

$$f_2\approx M_T a(a+b)\dot{p}\dot{r}-\bar{g}\dot{p}\dot{r}-M_T gb\alpha \tag{39}$$

$$f_3\approx-\left[\bar{g}+M_T a(a+b)\dot{r}\right]\dot{p}\dot{\alpha}-\left[M_T a(a+b)+2M_T b(a+b)\right]\dot{p}\dot{\alpha}\approx 0 \tag{40}$$

In addition, the term $M_{31}f_1$ in the third equation (35) can be neglected, since:

$$M_{31} f_1 \approx -\left[\bar{g} + M_T b(a+b)\right] \alpha \bar{g} \dot{r} \dot{\alpha} \approx 0 \tag{41}$$

Taking into account the approximations given by Eqs (36)-(41), the mathematical model of the wheel around a stable vertical rolling motion can be simplified as follows:

$$\frac{d^2 p}{dt^2} \approx \frac{f_1}{M_{11}} \;\; ; \;\; -\frac{d^2 \alpha}{dt^2} \approx \frac{f_2}{M_{22}} \;\; ; \;\; \frac{d^2 r}{dt^2} \approx 0 \tag{42}$$

From the third equation of (42) it is deduced that the angular velocity of the wheel is approximately constant. Furthermore, the system of differential equations (42) is linear according to Eqs (37)-(41). Introducing $\dot{r}_0 \approx Cte$ for the angular velocity of the wheel, Eqs (42) can be rewritten in the form:

$$\left.\begin{aligned} \frac{d^2 p}{dt^2} &= -\frac{\bar{g} \dot{r}_0}{M_{11}} \frac{d\alpha}{dt} \\ -\frac{d^2 \alpha}{dt^2} &= \left[\frac{M_T a(a+b) - \bar{g}}{M_{22}}\right] \dot{r}_0 \frac{dp}{dt} - \frac{M_T g b}{M_{22}} \alpha \end{aligned}\right\} \tag{43}$$

Assuming that $\dot{p}(0) = 0$ and $\alpha(0) = \alpha_0$ for *t=0*, the value of *dp/dt* can be deduced from the first equation of (43) and it can be substituted in the second equation of (43) to obtain that:

$$\frac{d^2 \alpha}{dt^2} + \left\{\frac{\bar{g}\left[\bar{g} - M_T a(a+b)\right] \dot{r}_0^2}{M_{11} M_{22}} - \frac{M_T g b}{M_{22}}\right\} \alpha = \frac{\bar{g}\left[\bar{g} - M_T a(a+b)\right] \dot{r}_0^2}{M_{11} M_{22}} \alpha_0 \tag{44}$$

From Eq (44) it is deduced that the following inequality must be fulfilled to obtain a stable system:

$$\dot{r}_0 > \sqrt{\frac{M_T g b M_{11}}{\bar{g}\left[\bar{g} - M_T a(a+b)\right]}} \tag{45}$$

where the term inside the square root is always positive, since $\bar{g} > M_T a(a+b)$ (see Eqs (13) and (37)). Equation (45) provides a lower limit for the angular velocity of the wheel to achieve stability, but it does not provide an upper limit for the angular velocity. To overcome this inconvenience, Eqs (44) and (45) allow to deduce the angular frequency associated to the wheel vibration motion as:

$$\omega_n = \sqrt{\frac{1}{M_{22}}\left\{\frac{\bar{g}\left[\bar{g} - M_T a(a+b)\right]\dot{r}_0^2}{M_{11}} - M_T g b\right\}} \tag{46}$$

Considering that the polar moment of inertia of the wheel is C_p (without taking into account the mass M_1 of the servomechanisms), the stability will be assured when the gyroscopic torque due to the rolling motion of the wheel (with angular velocity $\dot{r}_0$) compensates the gravity torque. Consequently, it follows that:

$$C_p \dot{r}_0 \omega_n = M_T g b \alpha \;\; ; \;\; C_p = M\left(b^2 + \frac{3}{2}a^2\right) \tag{47}$$

Eqs (46) and (47) lead to a four order equation which can be solved assuming that the term $\left(M_T g b \alpha / C_p\right)^2$ is negligible, which allows to deduce that the angular velocity of the wheel to obtain a stable rolling motion is given by:

$$\dot{r}_0 = \sqrt{\frac{M_T g b M_{11} M_{22}}{\bar{g}\left[\bar{g} - M_T a(a+b)\right]}} \tag{48}$$

It is interesting to remark that, on the basis of the Newton-Euler equations for a torus, the following stability condition has been obtained in Ref [4]:

$$\dot{r}_0 > \sqrt{\frac{A_e M_T g b}{C_p\left[C_p + M_T (a+b)^2\right]}} \;\; ; \;\; A_e = \frac{M}{4}\left(2b^2 + 5a^2\right) \tag{49}$$

where A_e and C_p are the equatorial and polar moments of inertia respectively. From Eq (49) it follows that $\dot{r}_0 > 2.6713$ rad/s, which is a clearly smaller value than the values

4.9769 and 8.4607 rad/s respectively deduced from Eqs (45) and (48). Finally, it is interesting to remark that the value of $\dot{r}_0$ can be much smaller than the values deduced from Eqs (45) and (48) when the wheel is actuated by control torques, as it will be analyzed in the next section. It should be noticed that the previous values for the angular velocity of the wheel deduced from Eqs (46), (48)-(49) are valid under ideal conditions of rolling without slipping. In fact, as long as the value of $\dot{r}_0$ given by Eq(48) becomes high, the lateral reaction force μ (see Figs 1 and 2) can be very high and consequently other phenomena that have not been considered in our model -such as sliding and pivoting- may appear. To investigate this issue, the mathematical model of the wheel is solved numerically by introducing the following state variables:

$$\begin{gathered} x_1(t)=p(t)\ ,\ x_2(t)=\dot{p}(t)\ ,\ x_3(t)=q(t)\ ,\ x_4(t)=\dot{q}(t)\ ,\ x_5(t)=r(t)\ ,\ x_6(t)=\dot{r}(t) \\ x_7(t)=x(t)\ ,\ x_8(t)=\dot{x}(t)\ ,\ x_9(t)=y(t)\ ,\ x_{10}(t)=\dot{y}(t) \end{gathered} \tag{50}$$

Assuming that M_r is a constant rolling torque that accounts for the deformation at the contact point between the wheel and the supporting plane, Eqs (16), (17), (29), (30), (34), (35) and (50) allow to obtain the following nonlinear differential equations:

$$\left.\begin{aligned} \dot{x}_1 &= x_2 \\ \dot{x}_2 &= \frac{M_{22}M_{33}}{\Delta}\,f_1 - \frac{M_{13}M_{22}}{\Delta}\left[\,f_3 + M_r\,\right] \\ \dot{x}_3 &= x_4 \\ \dot{x}_4 &= \frac{f_2}{M_{22}} \\ \dot{x}_5 &= x_6 \\ \dot{x}_6 &= -\frac{M_{22}M_{31}}{\Delta}\,f_1 + \frac{M_{11}M_{22}}{\Delta}\left[\,f_3 + M_r\,\right] \\ \lambda &= \left(\,f_{x2}\cos x_1 + f_{y2}\sin x_1\right) + \left(\,f_{x1}\cos x_1 + f_{y1}\sin x_1\right) \\ \mu &= \left(-f_{x2}\sin x_1 + f_{y2}\cos x_1\right) + \left(-f_{x1}\sin x_1 + f_{y1}\cos x_1\right) \\ \dot{x}_7 &= x_8 \\ \dot{x}_8 &= -b\left[-\dot{x}_2\cos x_1\cos x_3 + \dot{x}_4\sin x_1\sin x_3 + \left(x_2^2 + x_4^2\right)\sin x_1\cos x_3\right] \\ &\quad +2bx_2x_4\cos x_1\sin x_3 + \left(\lambda/M_T\right)\cos x_1 - \left(\mu/M_T\right)\sin x_1 \\ \dot{x}_9 &= x_{10} \\ \dot{x}_8 &= b\left[\,\dot{x}_2\sin x_1\cos x_3 + \dot{x}_4\cos x_1\sin x_3 + \left(x_2^2 + x_4^2\right)\cos x_1\cos x_3\,\right] \\ &\quad -2bx_2x_4\sin x_1\sin x_3 + \left(\lambda/M_T\right)\sin x_1 + \left(\mu/M_T\right)\cos x_1 \end{aligned}\right\} \tag{51}$$

The Euler angles *(p,q,r)* can be obtained by integrating Eqs (51), whereas the reaction forces λ and μ can be deduced from Eqs (28-30). On the other hand, the position of the contact point *(x,y)* between the wheel and the plane can be obtained through Eqs (16), (17) and (30). The initial conditions for Eqs (51) are chosen assuming that the nonholonomic constraints given by Eqs (3) are verified at $t = 0$. The Runge-Kutta-Fehlberg integration method has been used with simulations steps between 0.0001 and 0.001 s. It should be noticed that the problem of the integrability of Eqs (51) is not considered in this work since it has already been discussed for a rolling disk in Refs [29-32].

Fig 3 shows the simulation results obtained for the wheel and assuming that the rolling torque M_r is zero. The parameter values are indicated in the legend of Fig 1 and the initial coordinates of the contact point between the wheel and the horizontal plane are arbitrarily taken as (0.2, 0.5) m. The initial value of the precession angle is arbitrarily chosen as 50º ($p(0) = 0.8727\ rad$), whereas $dp(0)/dt = 0.05$ rad/s, $\alpha_0 = -10^{-4}$ rad ($q(0) = \pi/2 - 10^{-4}$) and $r(0) = 0$.

Taking $\dot{r}_0 = 10$ rad/s > 8.4607 rad/s, Fig 3 a) shows that the trajectory of the contact point between the wheel and the plane is close to a straight line, which is in accordance with the previous hypothesis of a very small angular precession velocity ($\dot{p} \approx 0$). Fig 3 b) shows that the angular velocity of the wheel changes very slowly, so the angular acceleration of the wheel can be neglected in accordance with the previous approximations. The reaction forces *(λ, μ)* are plotted in Fig 3 c), which shows that the reaction force λ is very small whereas the lateral reaction force μ increases with time, and therefore the wheel will be ultimately unstable for high values of μ (see Figs 1 and 2). The results of Fig 3 d) show the nonholonomic conditions as a function of the time, which are defined from Eqs (3) as follows:

$$\left.\begin{aligned} Nh_1 &= \dot{x} + \dot{r}\left(b + a\sin q\right)\cos p - a\dot{q}\sin p \\ Nh_2 &= \dot{y} + \dot{r}\left(b + a\sin q\right)\sin p + a\dot{q}\cos p \end{aligned}\right\} \tag{52}$$

If the condition of rolling without slipping had been fulfilled, Nh_1 and Nh_2 would have been equal to zero (despite the unavoidable numerical errors associated to the

integration process). However, Nh_1 and Nh_2 grow with time in the case shown in Fig 3 d). Consequently, after a long period of time Nh_1 and Nh_2 will reach high values and thus the hypothesis of rolling without sliding stops being valid, i.e. the mathematical model given by Eqs (51) looses its validity.

Figure 3

Fig 4 shows the effect of the rolling torque M_r due to the deformation of the wheel rolling on the horizontal plane. Fig 4 a) shows a plot of the coordinates of the contact point C (see Figs 1 and 2) as a function of the time, where the time t_2 denotes the instant at which the wheel lies on the plane at rest. Fig 4 b) shows the velocities associated to the coordinates *x(t)* and *y(t)* (see Eq (12) for the kinetic energy of the wheel). The trajectory of the contact point of the wheel in the horizontal plane is plotted in Fig 4 c), and the precession angle is plotted in Fig 4 d). It should be noted that, for $t \geq t_2$, the precession velocity is zero and the precession angle remains unaltered.

Figure 4

The leaning angle and velocity plotted in Fig 5 a) are both zero (wheel lying at rest on the plane) for $t \geq t_2$. On the other hand, Fig 5 b) shows that the angular velocity of the wheel decreases with time due to the effect of the rolling torque M_r, and approximately at $t = t_2$ the wheel looses its stability and begins to drop on the horizontal plane. The drop time is approximately given by $t_2 - t_1 \approx 0.3110$ s. Fig 5 c) shows that the reaction forces between the wheel and the plane increase very quickly when the wheel starts to drop. Fig 5 d) shows that the nonholonomic conditions (Eq (52)) are not fulfilled when the wheel drops, i.e. the hypothesis of rolling without sliding does not hold.

Figure 5

To verify that the numerical computations lead to physically meaningful results, Fig 6 shows the kinetic energy T, the potential energy V, the total energy E and the energy WM_r associated to the rolling torque M_r, all of them plotted against the time. These energies are used to verify the energy balance, and are defined at different instants of time as follows:

$$E(0) = T(0) + V(0)$$
$$E(t_1) = WM_r(t_1) + WM_{rd} + T(t_1) + V(t_1) - V(t_2) \tag{53}$$
$$WM_r(t_1) = \int_0^{t_1} M_r \omega_r(\tau)\, d\tau \;\; ; \;\; WM_{rd} = \int_{t_1}^{t_2} M_r \omega_r(\tau)\, d\tau \;\; ; \;\; \omega_r(t) = \frac{dr(t)}{dt}$$

where *E(0), K(0), V(0)* and $E(t_1)$, $K(t_1)$, $V(t_1)$ are the total, kinetic and potential energies at $t = 0$ and $t = t_1$ respectively. The term WM_r is the energy disipation due to the rolling torque between $t = 0$ and $t = t_1$, whereas WM_{rd} is the energy disipation due to the drop process of the wheel between $t = t_1$ and $t = t_2$. The instant $t_1 = 18.9250$ s is calculated in the simulation process assuming that the wheel drops when the leaning angle *q(t)* is higher than 20º, while the instant $t_2 = 19.2630$ s is the one at which $q(t) = 0$ (see Fig 5 a)). The total energy E(0) is calculated from Eqs (12)-(14) and from the initial conditions, which are defined as:

$$x_0 = \begin{bmatrix} p & \dot{p} & q & \dot{q} & r & \dot{r} & x & \dot{x} & y & \dot{y} \\ 50^\circ & 0 & (\pi/2)+10^{-4} & 0 & 0 & 8.4607 & 0.5 & -2.1754 & 0.2 & -2.5925 \end{bmatrix} \tag{54}$$

where the values of $\dot{x}$ and $\dot{y}$ are deduced from the nonholonomic constraints given by Eqs (3). The values obtained for *T(0), V(0)* and *E(0)* are 75.8781, 31.3600 and 107.2381 joules respectively. Similarly the values obtained for $WM_r(t_1)$, WM_{rd}, $T(t_1)$, $V(t_1)$ and $V(t_2)$ at $t_1 = 18.952$ s are 41.2656, 0.6994, 42.8367, 29.9483 and 7.8400 joules respectively. The sum of such energies is equal to 106.9101 joules, which is very close to the value of $E(0) = 107.2381$ joules (with a relative error of only 0.3058 %) in accordance with Eq (53). It should be noticed that $V(t_2) = M_T ga = 7.8400$ joules is the residual potential energy of the wheel when it remains at rest.

Figure 6

4 Stabilization torque and circular trajectories of the wheel

The discussion of the previous section clearly shows that the wheel is highly unstable, so a stabilizing torque is required to maintain a stable vertical rolling motion. On the other hand, a small rolling angular velocity is desirable to achieve the fulfillment

of the rolling without slipping condition. Consequently, we shall define a stabilizing torque around the leaning angle *q(t)* as follows:

$$M_{sq}(t)=\begin{cases} f_a M_T gb\cos q(t)+K_p\left[\pi/2+La-q(t)\right] & \text{if} \quad q(t)>\pi/2+La \\ f_a M_T gb\cos q(t) & \text{if} \quad \pi/2-La<q(t)<\pi/2+La \\ f_a M_T gb\cos q(t)+K_p\left[\pi/2-La-q(t)\right] & \text{if} \quad q(t)<\pi/2-La \end{cases} \tag{55}$$

where $f_a > 0$ is a factor to compensate the gravity torque, *La* is a limit angle whose value is chosen between ± 1º and K_p is a tunable constant whose value is chosen between 10 and 100 Nm. Next, we are going to demonstrate the suitability of the torque defined in Eq (55) to achieve stability.

Taking into account the approximations of Eq (36), introducing the stabilizing torque defined by Eq (55) and assuming that $\dot{r} \approx \dot{r}_0$, Eq (39) can be written as:

$$f_2 \approx \begin{cases} M_T a(a+b)\,\dot{p}\dot{r}_0 - \bar{g}\dot{p}\dot{r}_0 - M_T gb\alpha + f_a M_T gb\alpha + K_p\left[\alpha \pm La\right] \\ \qquad -\alpha(t) > La \ \text{ or } \ -\alpha(t) < -La \\ M_T a(a+b)\,\dot{p}\dot{r}_0 - \bar{g}\dot{p}\dot{r}_0 - M_T gb\alpha + f_a M_T gb\alpha \ ; \text{for } K_p = 0 \end{cases} \tag{56}$$

On the other hand, from Eqs (42)-(44) it is deduced that:

$$\frac{d^2\alpha}{dt^2}=\begin{cases} -\left\{\dfrac{\bar{g}\left[\bar{g}-M_T a(a+b)\right]\dot{r}_0^2}{M_{11}M_{22}}+\dfrac{K_p-(1-f_a)M_T gb}{M_{22}}\right\}\alpha+\dfrac{\bar{g}\left[\bar{g}-M_T a(a+b)\right]\dot{r}_0^2}{M_{11}M_{22}}(\alpha_0 \pm L_a) \\ -\left\{\dfrac{\bar{g}\left[\bar{g}-M_T a(a+b)\right]\dot{r}_0^2}{M_{11}M_{22}}-\dfrac{(1-f_a)M_T gb}{M_{22}}\right\}\alpha+\dfrac{\bar{g}\left[\bar{g}-M_T a(a+b)\right]\dot{r}_0^2}{M_{11}M_{22}}\alpha_0 \quad \text{for } K_p=0 \end{cases} \tag{57}$$

Let us assume that:

$$\begin{gathered} K_p > 0 \ \text{ and } \ K_p > (1-f_a)M_T gb \ ; \ 0 < f_a \le 1 \\ K_p = 0 \ \text{ and } \ f_a \ge 1 \end{gathered} \tag{58}$$

From Eq (57) it can be deduced that the values of K_p and f_a given in Eq (58) lead to an unconditionally stable system, so Eq (54) can be considered as an adequate stabilizing torque for the rolling wheel.

Once the stabilizing torque is defined, the conditions to obtain a circular trajectory can be analyzed from the nonholonomic constraints given by Eqs (3). For this purpose, we assume that the nonholonomic conditions given by Eqs (52) are exactly verified and therefore $Nh_1 = 0$ and $Nh_2 = 0$. Besides, appropriate torques around the Euler angles *(p, q ,r)* are applied at an arbitrary instant $t = t_0$ so that the following conditions are fulfilled:

$$\dot{p}(t) = \dot{p}_0 \; ; \; q(t) = q_0 \Rightarrow \dot{q}(t) = 0 \; ; \; \dot{r}(t) = \dot{r}_0 \tag{59}$$

where $\dot{p}_0$, q_0 and $\dot{r}_0$ are constants. From Eqs (52) and (59) it is deduced that:

$$\begin{gathered} \dot{x}(t) = K_1 \cos p(t) \;\; ; \;\; \dot{y}(t) = K_1 \sin p(t) \\ K_1 = -\dot{r}_0 \left(b + a \sin q_0 \right) \;\; ; \;\; p(t) = p_0 + \dot{p}_0 \left(t - t_0 \right) \end{gathered} \tag{60}$$

where p_0 is the precession angle of the wheel at $t = t_0$. Consequently, the coordinates of the contact point *C* of the wheel describe a circular trajectory whose radius and center coordinates can be calculated through the following procedure. By integrating Eqs (60) it is deduced that:

$$\begin{gathered} x(t) - K_{x0} = K_1 \left\{ \frac{\cos p_0}{\dot{p}_0} \sin\left[\dot{p}_0 \left(t - t_0 \right) \right] + \frac{\sin p_0}{\dot{p}_0} \cos\left[\dot{p}_0 \left(t - t_0 \right) \right] \right\} \\ y(t) - K_{y0} = K_1 \left\{ \frac{\sin p_0}{\dot{p}_0} \sin\left[\dot{p}_0 \left(t - t_0 \right) \right] - \frac{\cos p_0}{\dot{p}_0} \cos\left[\dot{p}_0 \left(t - t_0 \right) \right] \right\} \\ K_{x0} = x_0 - \frac{K_1}{\dot{p}_0} \sin p_0 \;\; ; \;\; K_{y0} = y_0 + \frac{K_1}{\dot{p}_0} \cos p_0 \end{gathered} \tag{61}$$

and by eliminating the time between Eqs (61) it is deduced that:

$$\left[x(t) - K_{x0} \right]^2 + \left[y(t) - K_{y0} \right]^2 = \left(\frac{K_1}{\dot{p}_0} \right)^2 \tag{62}$$

which is the equation of a circle with radius $\left|K_1/\dot{p}_0\right|$ and center coordinates *(K_{x0}, K_{y0})*. Next, from Eqs (31) and (35) it is possible to determine the necessary torques to obtain a circular trajectory. Considering the stabilization torque $M_{sq}(t)$ given by Eq (55) for $t \leq t_0$, and denoting by $M_p(t)$, $M_q(t)$ and $M_r(t)$ the torques around the Euler angles p , q and r for $t > t_0$, it is deduced that:

$$\left.\begin{aligned} \frac{d^2p(t)}{dt^2} &= \frac{M_{22}(t)}{\Delta(t)}\left[M_{33}(t)\,f_1(t) - M_{13}(t)\,f_3(t)\right] \\ \frac{d^2q(t)}{dt^2} &= \frac{f_2(t)+M_{sq}(t)}{M_{22}(t)} \qquad \text{for } t \leq t_0 \\ \frac{d^2r(t)}{dt^2} &= \frac{M_{22}(t)}{\Delta(t)}\left[-M_{31}(t)\,f_1(t) + M_{11}(t)\,f_3(t)\right] \end{aligned}\right\} \tag{63}$$

$$\left.\begin{aligned} \frac{d^2p(t)}{dt^2} &= \frac{M_{22}(t)}{\Delta(t)}\left\{M_{33}(t)\left[f_1(t)+M_p(t)\right] - M_{13}(t)\left[f_3(t)+M_r(t)\right]\right\} \\ \frac{d^2q(t)}{dt^2} &= \frac{f_2(t)+M_q(t)}{M_{22}(t)} \qquad \text{for } t > t_0 \\ \frac{d^2r(t)}{dt^2} &= \frac{M_{22}(t)}{\Delta(t)}\left\{-M_{31}(t)\left[f_1(t)+M_p(t)\right] + M_{11}(t)\left[f_3(t)+M_r(t)\right]\right\} \end{aligned}\right\} \tag{64}$$

Consequently, the system given by Eqs (63) is unconditionally stable. On the other hand, from Eqs (59) and (64) it is deduced that the required conditions to obtain a circular trajectory are given by:

$$M_p(t) = -f_1(t) \;\; ; \;\; M_q(t) = -f_2(t) \;\; ; \;\; M_r(t) = -f_3(t) \tag{65}$$

The investigation of the circular trajectories is carried out through the simulation of Eqs (50) by using the fourth-order Runge-Kutta method with integration steps between 0.001 s and 0.004 s, and with initial conditions given by:

$$x_0 = \begin{bmatrix} p & \dot{p} & q & \dot{q} & r & \dot{r} & x & \dot{x} & y & \dot{y} \\ 50^\circ & 0.05 & (\pi/2)+10^{-2} & 10^{-3} & 0 & 0.5 & 0.5 & -0.1285 & 0.2 & -0.1533 \end{bmatrix} \tag{66}$$

where the values of $\dot{x}$ and $\dot{y}$ have been obtained from the nonholonomic constraints given by Eqs (3). Assuming that the rolling torque M_r is very small, the stabilizing

torque M_{sq} given by Eq (55) is applied and thus f_2 must be replaced by $f_2 + M_{sq}$ in Eqs (51). The application of such stabilizing torque M_{sq} allows to achieve stability even when the initial angular velocities are smaller than the values deduced from Eqs (45) and (48)-(49) (which are 4.9769, 8.4612 and 2.6713 rad/s respectively). Consequently, an arbitrary initial angular velocity of 0.5 rad/s is now chosen. The simulation time is 80 s, and for $t \leq t_{co}$ = 40 s the stabilizing torque given by Eq (55) is applied taking f_a = 1, La = 1º and K_p =50. The previous values ensure the fulfillment of Eqs (57) and (58), i.e. the system is unconditionally stable. For $t > t_{co}$, the torques given by Eqs (65) are applied so that Eqs (58) are fulfilled, and consequently the circular trajectory appears.

Figs 7 a) and 7 b) depict the coordinates and velocities associated to the trajectory of the contact point C, where sinusoidal oscillations appear due to the presence of a circular trajectory for $t > t_{co}$ = 40. Fig 7 c) shows the precession angle and its corresponding velocity, which is equal to 0.05 rad/s for $0 < t < t_{co}$ = 40 s (see Eq (66)) and it is set to 0.2 rad/s for $t \geq t_{co}$ = 40 s. Fig 7 d) shows that for $t < t_{co}$ = 40 s the leaning angle has maintained oscillations with a very small amplitude due to the stabilizing torque (compare with Fig 3 without stabilizing torque), whereas for $t \geq t_{co}$ the wheel remains stable with a circular trajectory as shown in Fig 8. The coordinates of the center of the circular trajectory have been obtained from the simulation results, and they are approximately equal to the values deduced from Eqs (61), in which x_0 and y_0 are the coordinates of contact point P at t_{co} = 40 s. On the other hand, denoting by $x(t)$ and $y(t)$ the coordinates of the contact point C between the wheel and the plane at a time instant t, the curvature radius of the trajectory of point P is calculated as:

$$r(t) = \frac{\left[\dot{x}^2(t) + \dot{y}^2(t)\right]^{3/2}}{\ddot{y}(t)\dot{x}(t) - \ddot{x}(t)\dot{y}(t)} \tag{67}$$

The mean value of $r(t)$ is 1.0009 m, which is almost equal to the value 1.0004 m obtained for the radius of the circumference through Eq (61) for $t_0 = t_{co}$.

Figure 7

Figure 8

Fig 9 a) shows that the reaction force λ is very small whereas the reaction force μ is oscillating for $t < t_{co} = 40$ s and it remains almost constant when the wheel reaches the circular trajectory for $t \geq t_{co} = 40$. Fig 9 b) shows that the nonholonomic conditions given by Eqs (52) are acceptably small to warrant that the wheel has an approximately pure rolling motion without slipping, so the simulation results are in accordance with the mathematical assumptions of the model. Another verification of the simulation results is plotted in Fig 9 c), where the reaction force μ and the centrifugal force $F_g(t)$ are plotted for $t \geq t_{co} = 40$ s. Taking into account that the radius described by the mass center of the wheel is $r(t) - b\cos q(t)$, the dynamical equilibrium around the circular trajectory implies that:

$$F_g(t) + \mu = 0 \Rightarrow M_T \dot{r}^2(t)\left[r(t) - b\cos q(t)\right] + \mu = 0 \tag{68}$$

as shown in Fig 9 c). Fig 9 d) shows the relative error between $F_g(t)$ and μ, which is another indirect verification of the accurateness of the simulation results.

Figure 9

Fig 10 a) shows that the variations of the angular velocity are very small for $t < t_{co} = 40$ s when the stabilizing torque given by Eq (55) is applied. Besides, the value of $\dot{r}$ is almost constant for $t \geq t_{co}$ in accordance with the condition to obtain a circular trajectory given by Eqs (59). Figs 10 b) and c) depict the stabilizing torque given by Eq (55) and the torques given by Eqs (65). It is important to remark that such torques are very small and thus it is not necessary to take into account their energy in the Lagrangian equation (Eq (15)).

Figure 10

5 Arbitrary trajectories for the wheel rolling on the horizontal plane

In this section we investigate how to obtain control torques around the Euler angles *(p,q,r)* so that the contact point *C* between the wheel an the horizontal plane tracks a prescribed trajectory, being the latter described by a moving point in the plane OXY (see Fig 1). The key point for this study is that the Lagrangian formulation given

by Eq (15) contains the velocities $\dot{x}$ and $\dot{y}$ associated to the trajectory of the contact point *C*. It must be emphasized that $\dot{x}$ and $\dot{y}$ can be respectively viewed as the projections of the contact point velocity onto the axes OX and OY in an hypothetical situation in which the wheel would have a pure translation motion without rolling on the OXYZ reference system.

It should be recalled that Eqs (55) and (63) allow to stabilize the rolling motion around the leaning angle. On the basis of Eqs (64) we shall add torques $M_{pt}(t)$, $M_{qt}(t)$ and $M_{rt}(t)$ to obtain the adequate values of the Euler angles (p,q,r) and their derivatives so that the contact point C tracks the trajectory of a moving point on the OXY plane defined by the following parametric equations:

$$x_d(t) = x_d(\bar{p},t)\ ;\ y_d(t) = y_d(\bar{p},t) \tag{69}$$

The symbol $\bar{p}$ denotes a vector parameter which depends on the curve form. Assuming that the first and second derivatives of $x_d(t)$ and $y_d(t)$ can be calculated from Eqs (69), the velocity $(\dot{x}_d, \dot{y}_d)$ and the acceleration $(\ddot{x}_d, \ddot{y}_d)$ will be regarded as known functions. For this purpose, Eqs (25) and (26) can be rewritten as:

$$\begin{aligned}\ddot{x} &= C_{xp}(p,q,r)\ddot{p} + C_{xq}(p,q,r)\ddot{q} + C_{xr}(p,q,r)\ddot{r} + C_x(p,q,r,\dot{p},\dot{q},\dot{r})\\ \ddot{y} &= C_{yp}(p,q,r)\ddot{p} + C_{yq}(p,q,r)\ddot{q} + C_{yr}(p,q,r)\ddot{r} + C_y(p,q,r,\dot{p},\dot{q},\dot{r})\end{aligned} \tag{70}$$

where C_{xp}, C_{xq}, C_{xr} and C_{yp}, C_{yq}, C_{yr} only depend on the Euler angles whereas C_x and C_y depend on the Euler angles and their first derivatives. Operating in Eqs (25) and (26) it is deduced that:

$$\begin{aligned}&C_{xp} = 0\ ;\ C_{xq} = a\sin p\ ;\ C_{xr} = -(b + a\sin q)\cos p\\ &C_x = -b\left(\dot{p}^2 \sin p\cos q + \dot{p}\dot{q}\cos p\sin q\right) - b\left(\dot{p}\dot{q}\cos p\sin q + \dot{q}^2\sin p\cos q\right) + \frac{1}{M_T} f_{x1}\end{aligned} \tag{71}$$

$$\begin{aligned}&C_{yp} = 0\ ;\ C_{yq} = -a\cos p\ ;\ C_{yr} = -(b + a\sin q)\sin p\\ &C_y = b\left(\dot{p}^2 \cos p\cos q - \dot{p}\dot{q}\sin p\sin q\right) - b\left(\dot{p}\dot{q}\sin p\sin q + \dot{q}^2\cos p\cos q\right) - + \frac{1}{M_T} f_{y1}\end{aligned} \tag{72}$$

where f_{x1} and f_{y1} are given by Eqs (29). Next, the functions $F_1(t)$ and $F_2(t)$ are defined as:

$$\left.\begin{aligned} F_1(t) &= -2\delta_x\omega_{nx}\dot{x}(t) - \omega_{nx}^2 x(t) + \ddot{x}_d(t) + 2\delta_x\omega_{nx}\dot{x}_d(t) + \omega_{nx}^2 x_d(t) \\ &\quad + \frac{\omega_{nx}^2}{\tau_{ix}}\int_0^t e_x(\tau)\,d\tau \;\;;\;\; e_x(t) = \left[x_d(t) - x(t)\right] \\ F_2(t) &= -2\delta_y\omega_{ny}\dot{y}(t) - \omega_{ny}^2 y(t) + \ddot{y}_d(t) + 2\delta_y\omega_{ny}\dot{y}_d(t) + \omega_{ny}^2 y_d(t) \\ &\quad + \frac{\omega_{ny}^2}{\tau_{iy}}\int_0^t e_y(\tau)\,d\tau \;\;;\;\; e_y(t) = \left[y_d(t) - y(\tau)\right] \end{aligned}\right\} \tag{73}$$

where $F_1(t)$ and $F_2(t)$ are forces per unit of mass whereas $e_x(t)$ and $e_y(t)$ are the errors associated to the difference between the coordinates of the desired trajectory $\left[x_d(t), y_d(t)\right]$ and the actual coordinates $\left[x(t), y(t)\right]$ of the contact point C between the wheel rolling and the supporting plane OXY (see Figs 1 and Fig 2). The parameters δ_x and δ_y are regarded as damping coefficients, whereas ω_{nx} and ω_{ny} will be considered as the natural oscillation frequencies. It should be noted that if we take $\delta_x = 0$ and $\delta_y = 0$ (i.e. when there is no damping) and we assume that $\tau_{ix} = \infty$ and $\tau_{iy} = \infty$, Eqs (73) are similar to the ones related to undamped oscillators.

Taking into account that C_{xp} and C_{yp} are zero, and assuming that the coordinates of the desired trajectory $\left[x_d(t), y_d(t)\right]$ as well as their derivatives $\left[\dot{x}_d(t), \dot{y}_d(t)\right]$, $\left[\ddot{x}_d(t), \ddot{y}_d(t)\right]$ are known, Eqs (70)-(73) can be written as follows:

$$\begin{bmatrix} \ddot{x}(t) \\ \ddot{y}(t) \end{bmatrix} = \begin{bmatrix} C_{xq} & C_{yr} \\ C_{yq} & C_{yr} \end{bmatrix} \begin{bmatrix} \ddot{q}(t) \\ \ddot{r}(t) \end{bmatrix} + \begin{bmatrix} C_x \\ C_y \end{bmatrix} + \begin{bmatrix} F_x(t)/M_T \\ F_y(t)/M_T \end{bmatrix} = \begin{bmatrix} F_1(t) \\ F_2(t) \end{bmatrix} \tag{74}$$

where the terms $F_x(t)$ and $F_y(t)$ have units of force and they arise from the application of the required torques M_{qF} and M_{rF} around the Euler angles (q, r) (which are generated by the internal servomechanisms of the wheel) to ensure that:

$$\ddot{x}(t) = F_1(t) \;\;;\;\; \ddot{y}(t) = F_2(t) \tag{75}$$

It should be noticed that $F_x(t)$ and $F_y(t)$ cannot be change the precession angle p, which is in accordance with the fact that the coefficients C_{xp} and C_{yp} are zero (see Eqs (70)-(72)) and thus the acceleration $\ddot{p}(t)$ does not appear in Eq (74). On the other hand, Eqs (73) and (75) allow to rewrite the error along the axis OX as:

$$\ddot{e}_x(t) + 2\delta_x \omega_{nx} \dot{e}_x(t) + \omega_{nx}^2 e_x(t) + \frac{\omega_{nx}^2}{\tau_{ix}} \int_0^t e_x(\tau)\, d\tau = 0 \tag{76}$$

Eq (76) has the structure of a classical proportional + integral + derivative PID controller [24-26]. Taking $\tau_{ix} = \infty$, $0 < \delta_x < 1$ and assuming that C_1 and φ are constants that depend on the initial conditions, the solution of the differential equation (76) is:

$$e_x(t) = C_1 \frac{\exp(-\delta_x \omega_{nx} t)}{\sqrt{1-\delta_x^2}} \sin\left[\omega_{nx}\sqrt{1-\delta_x^2}\, t + \varphi\right] \Rightarrow \lim_{t\to\infty} e_x(t) = 0 \tag{77}$$

The same reasoning can be made for the error along the OY axis, and consequently, the desired trajectory can be reached by means of an adequate choice of the parameters δ and ω_n for the axes OX and OY.

The effect of the integral action is a quick decrease of the error, although the reset time τ_{ix} cannot be arbitrarily chosen in this case. This assertion can be corroborated by analyzing the roots of the characteristic polynomial of Eq (76) once the integral term has been removed by differentiation. Taking into account the Routh stability criterion [34], for the equations along the axes OX and OY it can be deduced that:

$$0 < \frac{1}{\tau_{ix}} < 2\delta_x \omega_{nx} \Rightarrow \tau_{ix} > \frac{1}{2\delta_x \omega_{nx}} \;;\; 0 < \frac{1}{\tau_{iy}} < 2\delta_y \omega_{ny} \Rightarrow \tau_{iy} > \frac{1}{2\delta_y \omega_{ny}} \tag{78}$$

Once the control law has been corroborated, it is necessary to analyze whether the nonholonomic conditions given by Eqs (52) are fulfilled. For this purpose, let us assume that the leaning angle along a prescribed trajectory is defined by:

$$q(t)=\pi/2\pm\alpha+A_q\sin\omega_q t\Rightarrow\begin{cases}\dot{q}(t)=A_q\omega_q\cos\omega_q t\\ \ddot{q}(t)=-A_q\omega_q^2\sin\omega_q t\end{cases} \tag{79}$$

where α and A_q are small angles ($\alpha \approx 10^{-3}$, $A_q \approx 10^{-4}$ rad) whereas ω_q is an arbitrary frequency which can also be small. If the previous assumptions are verified, the nonholonomic conditions can be approximated as follows:

$$\left.\begin{aligned}\dot{x}(t)&\approx-\dot{r}(t)\left[b+a\sin q(t)\right]\cos p(t)\\ \dot{y}(t)&\approx-\dot{r}(t)\left[b+a\sin q(t)\right]\sin p(t)\end{aligned}\right\}\Rightarrow p(t)\approx\arctan\left[\frac{\dot{y}(t)}{\dot{x}(t)}\right]$$
$$\dot{p}(t)\approx\frac{\ddot{y}(t)\dot{x}(t)-\ddot{x}(t)\dot{y}(t)}{\dot{x}(t)^2+\dot{y}(t)^2} \tag{80}$$

In Eq (80) it must be taken into account that the term $\dot{x}^2+\dot{y}^2$ can be zero, as it occurs in trajectories with singular points such as the astroid. To avoid excessively high values, a maximum value $\dot{p}_{\max}$ is chosen for $\dot{p}$. Therefore, if $\dot{p}(t)<0$ and $\left|\dot{p}(t)\right|\geq\dot{p}_{\max}$ then the value $\dot{p}(t)=-\dot{p}(t-T)$ is chosen in the numerical integration process. Similarly, if $\dot{p}(t)>0$ and $\left|\dot{p}(t)\right|>\dot{p}_{\max}$, the value $\dot{p}(t)=\dot{p}(t-T)$ is chosen, where T is the simulation step. In addition, taking into account Eq (80), the value of $\dot{r}(t)$ is:

$$\dot{r}(t)\approx\frac{\dot{x}(t)\cos p(t)-\dot{y}(t)\sin p(t)}{b+a\sin q(t)} \tag{81}$$

The accelerations $\ddot{p}(t)$ and $\ddot{r}(t)$ can be calculated from Eqs (80) and (81), and taking into account the Eqs (64) the corresponding torques $M_{pt}(t)$, $M_{qt}(t)$ and $M_{rt}(t)$ to track a desired trajectory can be very approximately calculated. To investigate the previous facts, in Fig 11 we illustrate how the contact point C follows a curve with general parametric equations given by:

$$\begin{aligned}x_d(t)&=x_{dc}+r(K-1)\cos\omega t+r\cos\left[(K-1)\omega t\right]\\ y_d(t)&=y_{dc}+r(K-1)\sin\omega t+r\sin\left[(K-1)\omega t\right]\end{aligned} \tag{79}$$

which is an astroid curve with K = 3 peaks, r = 2, center coordinates (x_{dc}, y_{dc}) and ω = $3.3\omega_{min}$, where ω_{min} = 0.0785 rad/s is the minimum frequency to obtain a cycle during a the simulation time of t_m = 100 s with a simulation step of T = 0.005 s. Fig 11 a) shows the simulation results of the successive contact points between the wheel and the plane OXY.

Starting from the initial conditions given by Eqs (66), the wheel rolls during 20 s with a stabilizing torque defined by aL = 0.01º, K_p = 50, f_a = 1 according to Eq (55). For t > 20 s, the control law given by Eqs (73) is applied assuming $\delta_x = \delta_y$ = 0.9, ω_{nx} = ω_{ny} = 2.55 rad/s and $\tau_{ix} = \tau_{iy} = 10^{10}$, so the integral action is negligible and thus a high steady-state error appears. Fig 11 b) is obtained with the same parameter values but taking $\tau_{ix} = \tau_{iy}$ = 0.3 s, which are close to the stability limit τ_{iL} = 0.2174 s given by Eq (78). In this case, a large initial oscillation appears. Taking into account the previous considerations, the values $\delta_x = \delta_y$ = 0.9, $\omega_{nx} = \omega_{ny}$ = 2.55 rad/s and $\tau_{ix} = \tau_{iy}$ = 0.5 s will be used in the rest of the numerical simulations.

Figure 11

Next we shall investigate the way to obtain an astroid with four peaks assuming the velocities, accelerations and torques in accordance with the previous analytical results. Assuming the same initial conditions given by Eqs (66) and the same parameter values used to obtain the Fig 11, Fig 12 a) shows the coordinates of the contact point C between the wheel and the supporting plane OXY. It should be noted that the stabilization torque given by Eq (55) is only applied for t < 20 s, whereas the stabilizing torque together with the control law defined by Eqs (73) and (74) are applied for $t \geq 20$ s. As expected, the contact point of the wheel tracks the desired trajectory. At the arbitrary instant $t = t_2$ = 65 s, the control law given by Eq (73) is changed by the following one:

$$\left.\begin{aligned} F_{1s}(t) &= -2\delta_{xs}\omega_{nxs}\dot{x}(t) - \omega_{nxs}^2\left[x(t) - x_{set}\right] \\ F_{2s}(t) &= -2\delta_{ys}\omega_{nys}\dot{y}(t) - \omega_{nys}^2\left[y(t) - y_{set}\right] \end{aligned}\right\} \tag{80}$$

where δ_{xs} and δ_{ys} are the damping coefficients, ω_{nxs} and ω_{nys} are the natural oscillation frequencies and x_{set}, y_{set} are the coordinates of an arbitrary set point that will be reached by the wheel. Consequently, for t ≥ 65 s Eq (75) must be replaced by:

$$\ddot{x}(t) = F_{1s}(t) \;\; ; \;\; \ddot{y}(t) = F_{2s}(t) \tag{81}$$

Assuming that $\delta_{xs} = \delta_{ys} = 0.5$ (i.e. satisfying that $0 < \delta_{xs} < 1$ and $0 < \delta_{ys} < 1$) and taking $\omega_{nxs} = \omega_{nys} = 0.5$ rad/s, Eqs (80) and (81) allow to conclude that the origin (which has been selected as set point) is reached as shown in Figs 12 a) and b). Taking a maximum value of the angular precession velocity of 5 rad/s, Figs 12 c) and 12 d) respectively show the precession and the leaning angles, which are in accordance with Eqs (79) and (80). Fig 13 shows the graphic of the astroid together with the trajectory of the contact point C. It should be remarked that the trajectory for $0 \leq t < 20$ s is very approximately a circumference since $q(t) \approx \pi/2$ (see Eq (79)), $\dot{p}(t)$ is constant (see Fig 12 c)) and $\dot{r}(t)$ is also constant and equal to the initial value of 0.5 rad/s. Consequently, the conditions given by Eq (59) are fulfilled.

Figure 12

Figure 13

Fig 14 a) shows the precession torque $M_{pt}(t)$ and the pedaling torque $M_{rt}(t)$ that are necessary to generate the trajectory of the wheel, which have been deduced from Eqs (64) and (65) taking into account the accelerations deduced from Eqs (80) and (81) and assuming a maximum value of $\ddot{p}(t) = 20$ rad/s^2. It should be noticed that there is an abrupt change of the precession torque at the peaks of the trajectory, whereas the values of the precession torque are small in the zones between peaks. In Fig 14 b) the stabilizing and the leaning torques are plotted showing that they are very small when the set point has been reached. However, such torques are not exactly equal to zero since they are necessary to maintain the wheel in vertical position once the set point has been reached. Other stabilization methods can be found in Refs [13-15], [33].

Figure 14

Fig 15 a) shows the plots of the terms $F_x(t)$ and $F_y(t)$ deduced from Eqs (74), whereas Fig 15 b) depicts the torques $M_{rF}(t)$ and $M_{qF}(t)$ that give rise to $F_x(t)$ and $F_y(t)$. Projecting F_x and F_y in the direction of $\dot{q}$ (see Fig 2 a)) and denoting by γ the angle between GC and GP in Fig 1 b), it is deduced that:

$$\begin{aligned} M_{rF} &= \left(F_x \cos p + F_y \sin p\right) GC \cos\gamma = \left(F_x \cos p + F_y \sin p\right)\left(b + a \sin q\right) \\ M_{qF} &= \left(F_x \sin p - F_y \cos p\right) \sin q GC \cos\gamma = \left(F_x \sin p - F_y \cos p\right) \sin q \left(b + a \sin q\right) \end{aligned} \tag{82}$$

It should be noted that the values of $M_{rF}(t)$ and $M_{qF}(t)$ are small except at the trajectory peaks. In Fig 16 a), the angular velocity of the wheel is plotted showing that it is oscillating without sign changes when the wheel tracks the astroid curve, since the wheel makes several cycles before the occurrence of a trajectory change to reach the set point. Fig 16 b) shows admissible values for the constraint reaction forces λ and μ at the contact point C whereas Fig 16 c) shows the nonholonomic conditions given by Eqs (52), both of them as functions of the time. It should be noticed that such nonholonomic conditions are very small and consequently the hypothesis of rolling without slipping can be regarded as acceptable. Finally, the wheel remains at rest at approximately at $t_3 \approx$ 100 s, but with a small (stabilizing) oscillation around the leaning angle.

Figure 15

Figure 16

6 Conclusions

The controlled motion of a wheel rolling without slipping on a horizontal plane has been investigated in this paper. The first step in our analysis has consisted of deriving the nonholonomic constraints associated to a pure rolling motion. By introducing adequate reference frames, the kinetic energy of the wheel has been obtained as a function of the Euler angles and the coordinates of the contact point between the wheel and the supporting plane. The proposed procedure is completely general and can be extended to a wheel rolling on an arbitrary surface whose implicit equation is known.

The mathematical model of the wheel is deduced from the Euler equations by using the method of the undetermined Lagrange multipliers and the nonholonomic constraints, which lead to a system of five second-order nonlinear differential equations. By eliminating the equations associated to the coordinates of the contact point between the wheel and the supporting plane, the system is reduced to three second-order nonlinear differential equations that only involve the Euler angles. These equations have been used to deduce the lower bound for the angular velocity of the wheel and the stability conditions for the motion assuming rolling without slipping and without external torques. In addition, the presence of a friction torque has also been investigated showing how it alters the stability of the wheel. The fulfillment of the principle of energy conservation has allowed to corroborate the simulation results.

The simulation results have shown that the rolling motion of the wheel is highly unstable in the absence of control torques. Consequently, a torque for stabilizing the wheel around the leaning angle has been included in the mathematical model of the system, leading to an unconditionally stable system with a smaller angular velocity that fulfills the nonholonomic conditions. The appearance of a circular trajectory is investigated from the nonholonomic conditions, showing that the dynamic equilibrium between the centrifugal and reaction forces are verified and thus the circular trajectory is stable.

The procedure to track an arbitrary trajectory is investigated through the second derivatives of the coordinates associated to the trajectory and defined at the contact point between the wheel and the supporting plane. For this purpose, two additional torques around the leaning and pedaling angles have been included in system giving raise to the appearance of two terms F_x and F_y with dimensions of force in the mathematical model. These terms are calculated by canceling of the nonlinear terms of the axes OX-OY with control laws of PID type.

The verification of the nonholonomic conditions along the prescribed trajectory, -even with singular cusp points such as in astroid curves- is carried out assuming that the variation of the leaning angle around the equilibrium position is very small. Consequently it is possible to calculate the second derivative of the Euler angles and the corresponding control torques through the equations of the mathematical model.

The investigations of this paper can be extended in many directions. For example, is possible to consider the stability properties of a wheel rolling on an arbitrary surface, for which a unified procedure to determine both the nonholonomic constraints and the mathematical model of the system can be computationally implemented through the proposed method in the paper. Finally, it should be noted that the consideration of more complex control laws deduced from the differential geometry can provide other interesting dynamical behaviors.

Appendix

In this appendix we introduce the rotation matrices and their derivates with respect to time, which are necessary to obtain the kinetic energy of the wheel with respect to the inertial frame OXYZ shown Figs 1 and 2. It should first be recalled that from step iv) of section 2.1 it follows that:

$$\vec{r}_s(t) = \bar{R}_{pqr}\vec{r}_p(t) \tag{A1}$$

where $\bar{R}_{pqr}$ is the rotation matrix defined as a function of the Euler angles *(p,q,r)* as follows:

$$\bar{R}_{pqr} = \left[\mathrm{R}_{\mathrm{pqr}}(1) \quad \mathrm{R}_{\mathrm{pqr}}(2) \quad \mathrm{R}_{\mathrm{pqr}}(3)\right]$$

$$\mathrm{R}_{\mathrm{pqr}}(1) = \begin{bmatrix} \cos p\cos r - \sin p\cos q\sin r \\ \sin p\cos r + \cos p\cos q\sin r \\ \sin q\sin r \end{bmatrix};\ \mathrm{R}_{\mathrm{pqr}}(2) = \begin{bmatrix} -\cos p\sin r - \sin p\cos q\cos r \\ -\sin p\sin r + \cos p\cos q\cos r \\ \sin q\cos r \end{bmatrix} \tag{A2}$$

$$\mathrm{R}_{\mathrm{pqr}}(3) = \begin{bmatrix} \sin p\sin q \\ -\cos p\sin q \\ \cos q \end{bmatrix}$$

The derivative $\dot{R}_{pqr}$ of the rotation matrix with respect to time can be simplified by introducing the following notation:

$$\dot{R}_{pqr} = \dot{p}\bar{U}_{pqr} + \dot{q}\bar{V}_{pqr} + \dot{r}\bar{W}_{pqr} \begin{cases} \bar{U}_{pqr} = \begin{bmatrix} \mathrm{U}_{pqr}(1) & \mathrm{U}_{pqr}(2) & \mathrm{U}_{pqr}(3) \end{bmatrix} \\ \bar{V}_{pqr} = \begin{bmatrix} \mathrm{V}_{pqr}(1) & \mathrm{V}_{pqr}(2) & \mathrm{V}_{pqr}(3) \end{bmatrix} \\ \bar{W}_{pqr} = \begin{bmatrix} \mathrm{W}_{pqr}(1) & \mathrm{W}_{pqr}(2) & \mathrm{W}_{pqr}(3) \end{bmatrix} \end{cases} \tag{A3}$$

where the column vectors in Eq (A3) are given by:

$$\mathrm{U}_{pqr}(1) = \begin{bmatrix} -\cos p \cos q \sin r - \sin p \cos r \\ -\sin p \cos q \sin r + \cos p \cos r \\ 0 \end{bmatrix}; \mathrm{U}_{pqr}(2) = \begin{bmatrix} -\cos p \cos q \cos r + \sin p \sin r \\ -\sin p \cos q \cos r - \cos p \sin r \\ 0 \end{bmatrix}$$

$$\mathrm{U}_{pqr}(3) = \begin{bmatrix} \cos p \sin q \\ \sin p \sin q \\ 0 \end{bmatrix}$$

(A4)

$$\mathrm{V}_{pqr}(1) = \begin{bmatrix} \sin p \sin q \sin r \\ -\cos p \sin q \sin r \\ \cos q \sin r \end{bmatrix}; \mathrm{V}_{pqr}(2) = \begin{bmatrix} \sin p \sin q \cos r \\ -\cos p \sin q \cos r \\ \cos q \cos r \end{bmatrix}$$

$$\mathrm{V}_{pqr}(3) = \begin{bmatrix} \sin p \cos q \\ -\cos p \cos q \\ -\sin q \end{bmatrix} \tag{A5}$$

$$\mathrm{W}_{pqr}(1) = \begin{bmatrix} -\sin p \cos q \cos r - \cos p \cos r \\ \cos p \cos q \cos r - \sin p \sin r \\ \sin q \cos r \end{bmatrix}; \mathrm{W}_{pqr}(2) = \begin{bmatrix} \sin p \cos q \sin r - \cos p \cos r \\ -\cos p \cos q \sin r - \sin p \cos r \\ -\sin q \sin r \end{bmatrix}$$

$$\mathrm{W}_{pqr}(3) = \begin{bmatrix} 0 \\ 0 \\ 0 \end{bmatrix}$$

(A6)

Equations (A3)-(A6) can be used to calculate the kinetic energy of the wheel with respect to the inertial frame OXYZ.

References

[1] E. J. Routh, The Advanced Part of a Treatise on the Dynamics of a System of Rigid Bodies, sixth ed., MacMillan & Co., London, 1905.

[2] P. Appell, Traité de Mécanique Rationalle, Tome Deuxieme, Gauthier-Villars, Paris, 1953.

[3] E. T. Whittaker, A Treatise on the Analytical Dynamics of Particles and Rigid Bodies, Cambridge University Press, Cambridge, 1917.

[4] J. I. Neimark, N. A. Fufaev, Dynamics of Nonholonomic Systems, Translations of Mathematical Monographs, American Mathematical Society, 1972.

[5] L. A. Pars, A treatise on Analytical Dynamics, Reprint, Ox Bow Press, 1966.

[6] H. Cabanbes, Cours de Mecanique Generale, second ed., Dunod, Paris, 1966.

[7] F. Gantmacher, Lectures in Analytical Mechanics, Mir Publishers, Moscow, 1970.

[8] R. Abraham, J. Marsden, Foundations of Mechanics, second ed., Addison Wesley, Reading, MA, 1978.

[9] J. E. Marsden, T.S. Ratiu, Introduction to Mechanics and Symmetry, second ed., Springer, New York, 1999.

[10] R. Cushman, H. Duistermaat, J. Śniatycki, Geometry of Nonholonomically Constrained Systems, first ed., World Scientific Publishing, New Jersey, 2010.

[11] A. M. Bloch, M. Reyhanouglu, N. H. McClamroch, Control and stabilization of nonholonomic dynamic systems, IEEE T Automat. Contr. 37 (1992) 1746-1757

[12] F. Bullo, A. D. Lewis, Geometric Control of Mechanical Systems, first ed., Springer, New York, 2000.

[13] A. M. Bloch, Nonholonomic Systems and Control, first ed., Springer, New York, 2000.

[14] J. Cortés Monforte, Geometric, Control and Numerical Aspects of Nonholonomic Systems, first ed., Springer-Verlag, Berlin, Heidelberg, 2002.

[15] N. Chakraborty, A. Ghosal, Kinematics of wheeled mobile robots on uneven terrain, Mechanism and Machine Theory, 39 (2004) 1273–1287.

[16] R. Andrzejewski, J.Awrejcewicz, Nonlinear Dynamics of a Wheeled Vehicle, first ed., Springer, New York, 2005.

[17] W. Johnson, An elementary analysis of an energy absorbing device: The rolling torus load limiter Original, International Journal of Mechanical Sciences. 15 (1973) 357-366.

[18] W. Johnson, S. Reid, The rolling torus: Some elastic-plastic considerations, International Journal of Mechanical Sciences, 16 (1974) 45-62.

[19] Johnson, S.R. Reid, L.B. Singh, Experimental study of the rolling torus load limiter, International Journal of Mechanical Sciences, 17 (1975) 603-606.

[20] J.R. Barber, M. Ciavarella, L. Afferrante, A. Sackfield, Effect of small harmonic oscillations during the steady rolling of a cylinder on a plane, International Journal of Mechanical Sciences, 50 (2008) 1344-1353.

[21] J.P.Hambleton, A.Drescher, On modeling a rolling wheel in the presence of plastic deformation as a three- or two-dimensional process, International Journal of Mechanical Sciences, 51 (2009) 846-855.

[22] Y. Yavin, P. D. Kemp, Modelling and control of the motion of a rolling disk: effect of the motor dynamics on the dynamical model, Comput Methods Appl. Mech., 188 (2000) 613-624.

[23] Y. Yavin, Directional Control of the Motion of a Rolling Disk by Using an Overhead Rotor, Dynam Cont Dis Ser B, 8 (2001) 111-125.

[24] Y. Yavin, Modelling of the Motion of a Disk Rolling on a Torus, Mathematical and Computer Modelling 36 (2002) 831-837.
[25] Y. Ou, Y. Xu, Gyroscopically Stabilized Robot: Balance and Tracking, Int J Adv Robot Syst, 1 (2004) 23-32.
[26] Manuel F. Pérez Polo, Manuel Pérez Molina, Javier Gil Chica, Stabilization and positioning control of a rolling disk by using the Bogdanov–Takens bifurcation, Physica D 241 (2012) 1450–1469.
[27] P. P. Teodorescu, Mechanical Systems, Classical Models. Vol 3. Analytical Mechanics, first ed., Springer, 2002.
[28] K. Ogata, Modern Control Engineering, fourth ed., Prentice-Hall, New York, 2000.
[29] H. Cendra, V. Díaz, The Lagrange-D'Alambert-Poincaré Equations and Integrability for the Rolling Disk, Regul Chaotic Dyn, 11 (2006) 67-81.
[30] A. V. Borisov, I. S. Mamaev, A. A. Killin, Dynamics of Rolling Disk, Regul Chaotic Dyn, 8 (2003) 201-212.
[31] O. M. O'Reilly, The Dynamics of Rolling Disks and Sliding Disks, Nonlinear Dynam, 10 (1996) 287-305.
[32] M. Batista, Integrability of the motion of a rolling disk of finite thickness on a rough plane, Int J Nonlin Mech, 41 (2006) 850-859.
[33] P. Cieslak, T. Buratowski, T. Uhl, M. Giergiel, The mono-wheel robot with dynamic stabilisation, Robotics and Autonomous Systems 59 (2011) 611–619.

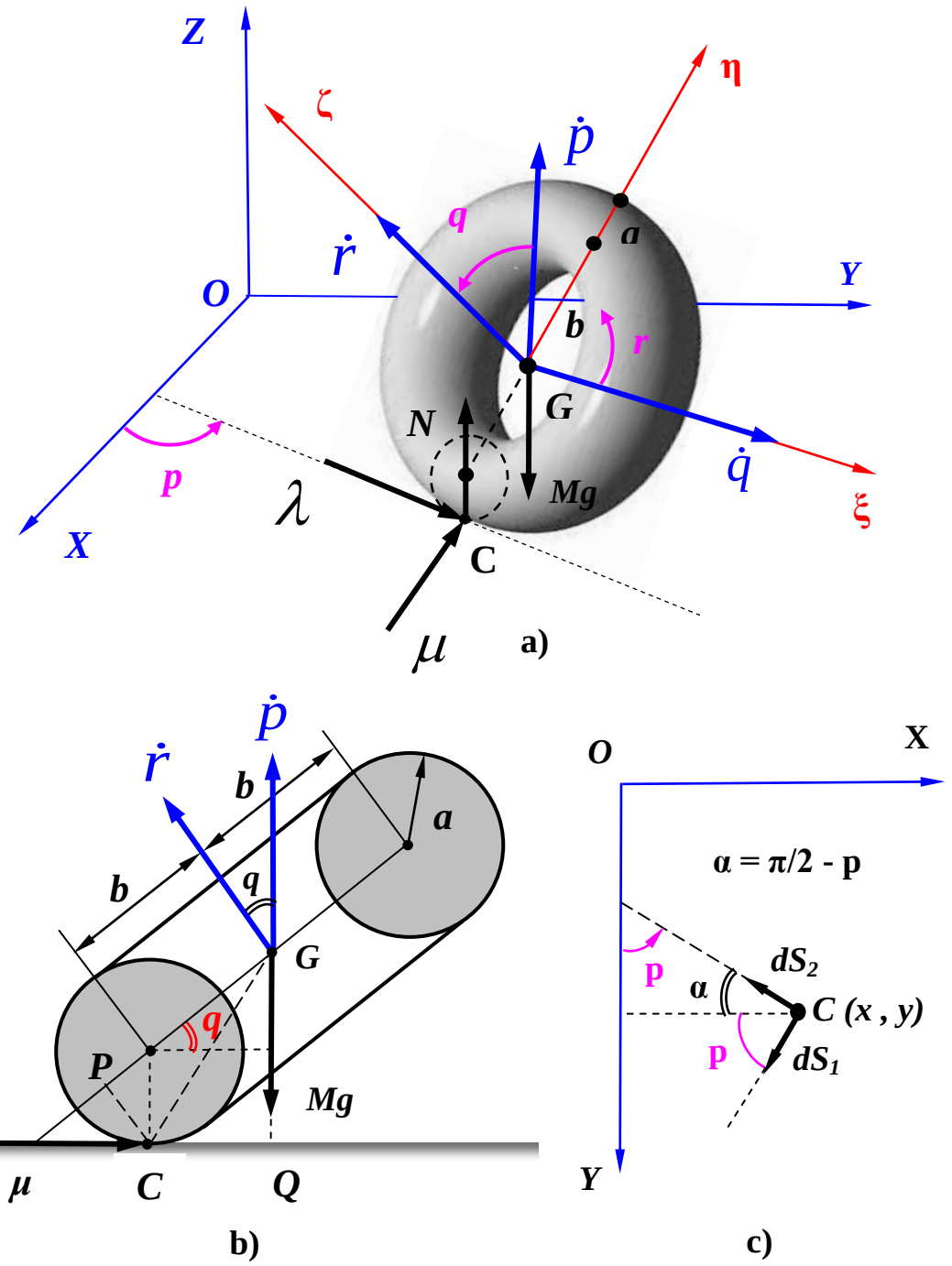
z
ζ
η
ṗ
q
ṙ
a
O
Y
b
r
G
N
Mg
q̇
p
λ
X
ξ
C
μ
a)
ṗ
ṙ
b
a
b
q
G
q
P
Mg
μ
C
Q
b)
O
X
α = π/2 - p
p
dS2
α
C (x , y)
p
dS1
Y
c)

Figure 1

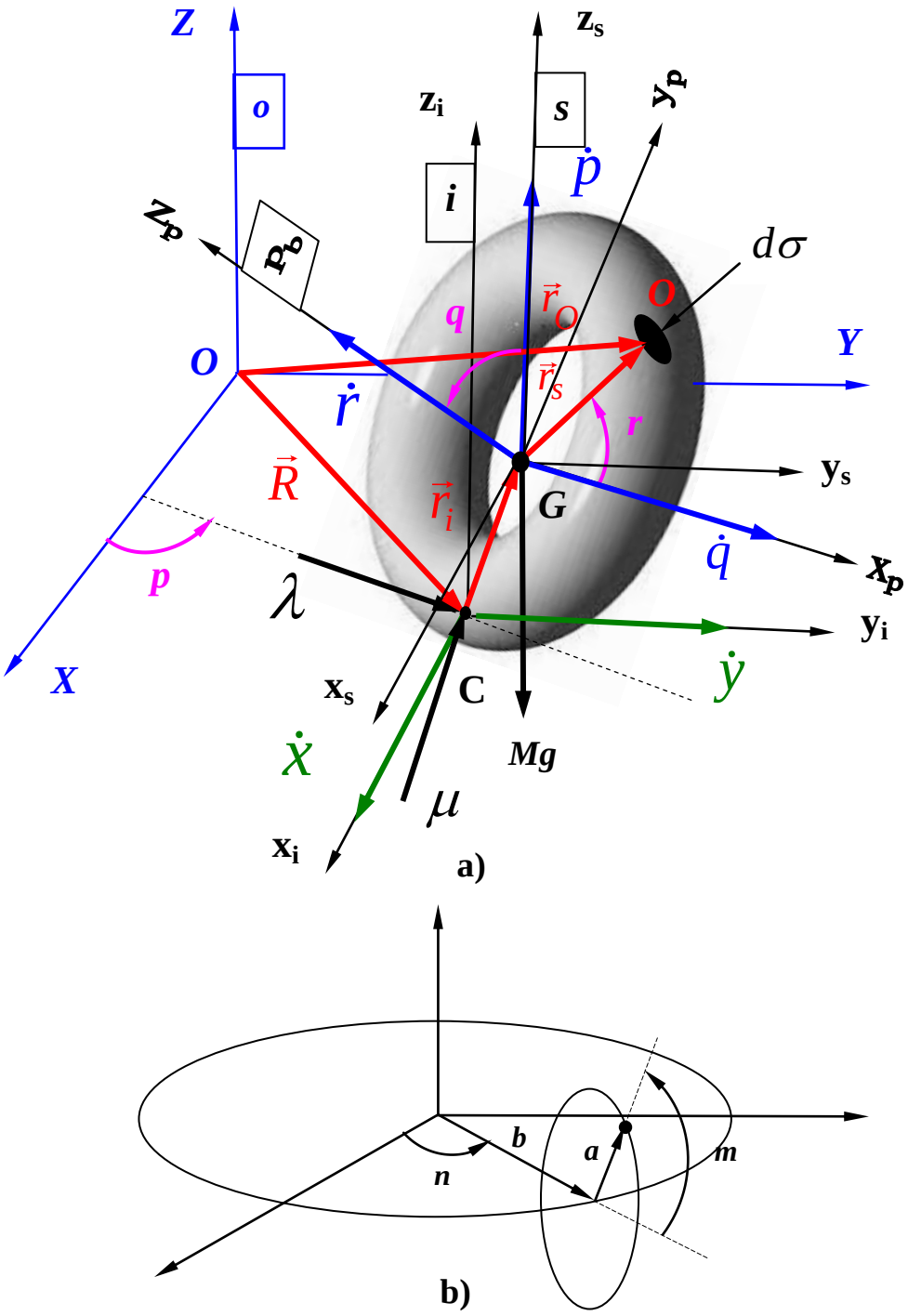
Z
o
z_i
z_s
s
i
y_p
p
x_p
dσ
O
q
r_O
Y
r_s
r
R
y_s
r_i
G
q̇
x_p
p
λ
y_i
X
x_s
C
ẏ
Mg
ẋ
μ
x_i
a)
b
a
m
n
b)

Figure 2

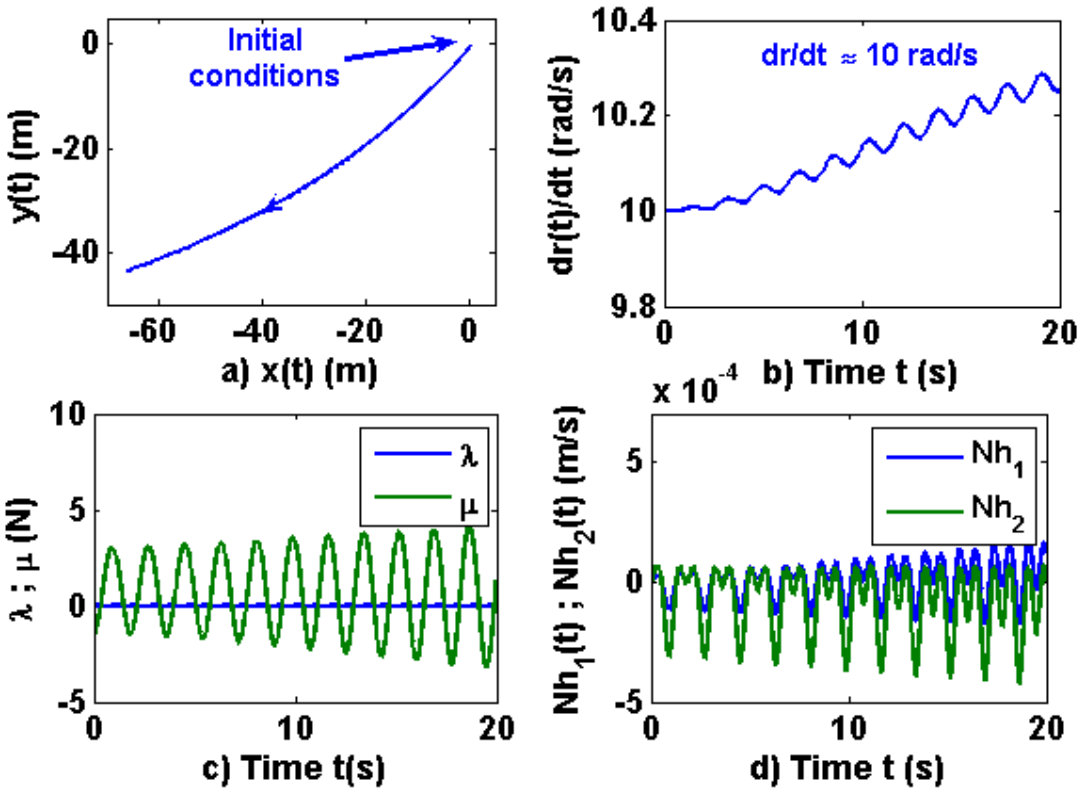
Initial conditions
y(t) (m)
a) x(t) (m)
dr/dt ≈ 10 rad/s
dr(t)/dt (rad/s)
b) Time t (s)
λ
μ
λ ; μ (N)
c) Time t(s)
x 10^-4
Nh1
Nh2
Nh1(t) ; Nh2(t) (m/s)
d) Time t (s)

Figure 3

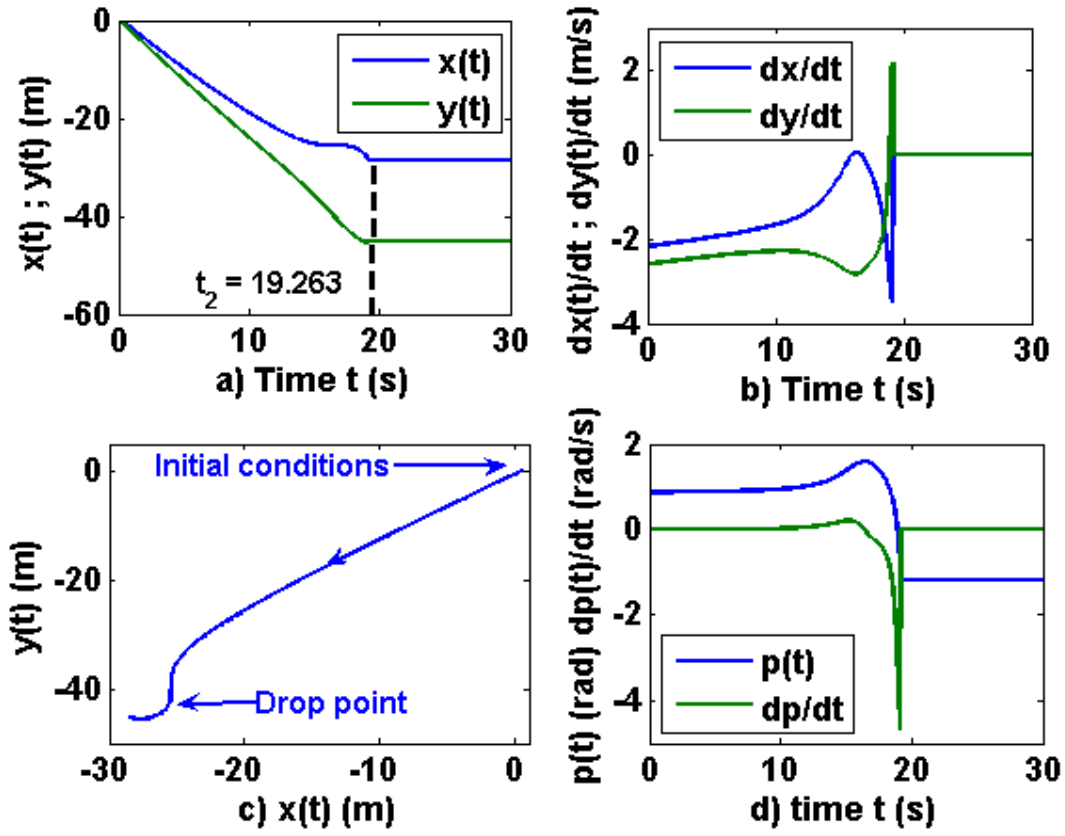
x(t)
y(t)
x(t) ; y(t) (m)
t2 = 19.263
a) Time t (s)
dx/dt
dy/dt
dx(t)/dt ; dy(t)/dt (m/s)
b) Time t (s)
Initial conditions
Drop point
y(t) (m)
c) x(t) (m)
p(t)
dp/dt
p(t) (rad) dp(t)/dt (rad/s)
d) time t (s)

Figure 4

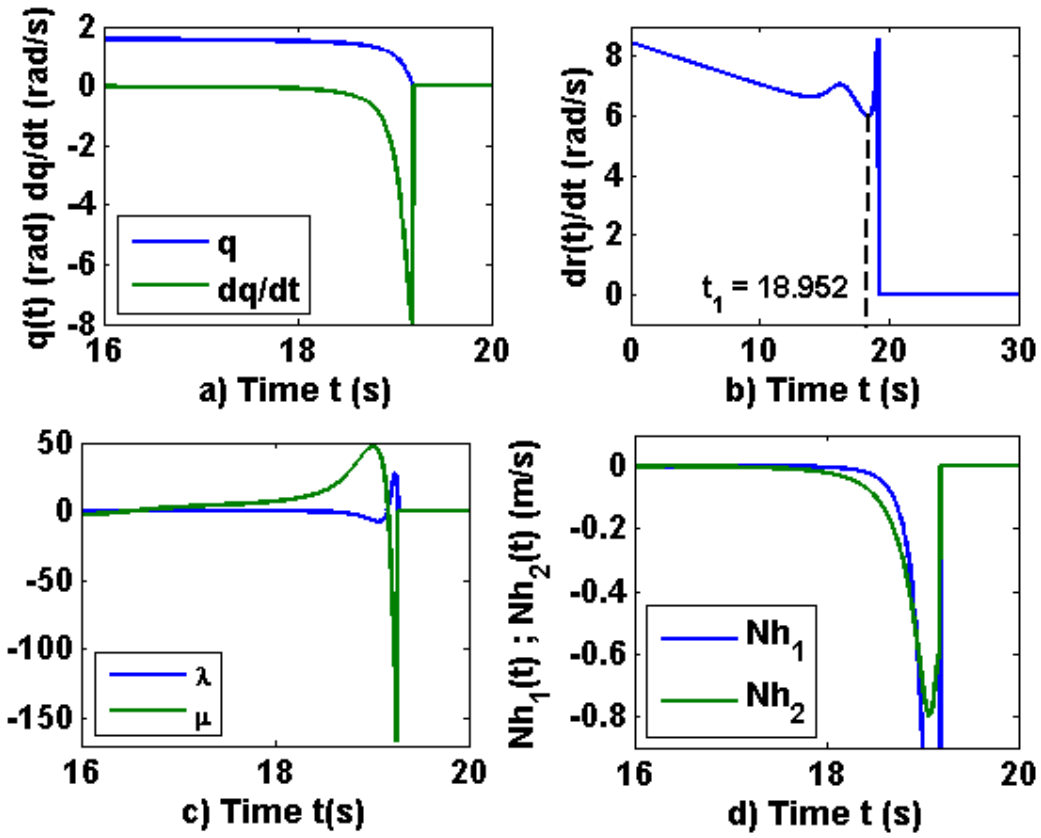
q(t) (rad) dq/dt (rad/s)
q
dq/dt
a) Time t (s)
dr(t)/dt (rad/s)
t1 = 18.952
b) Time t (s)
λ
μ
c) Time t(s)
Nh1(t) ; Nh2(t) (m/s)
Nh1
Nh2
d) Time t (s)

Figure 5

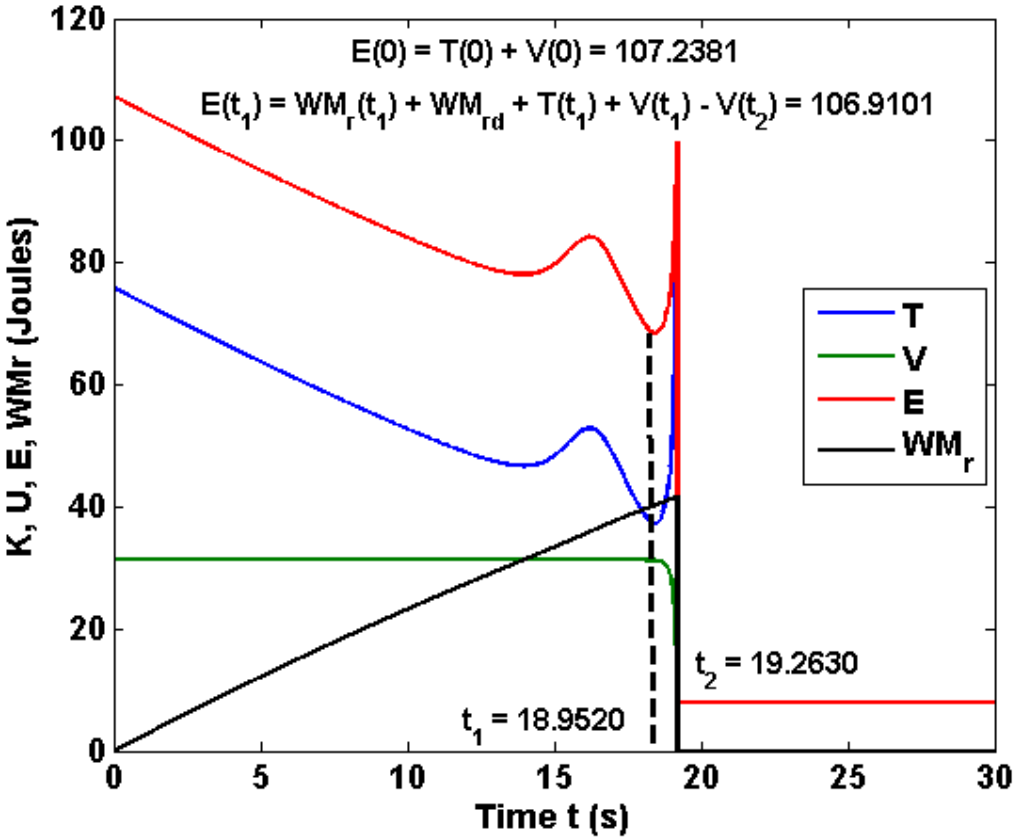
E(0) = T(0) + V(0) = 107.2381
E(t1) = WMr(t1) + WMrd + T(t1) + V(t1) - V(t2) = 106.9101
K, U, E, WMr (Joules)
Time t (s)
T
V
E
WMr
t1 = 18.9520
t2 = 19.2630
0
20
40
60
80
100
120
0
5
10
15
20
25
30

Figure 6

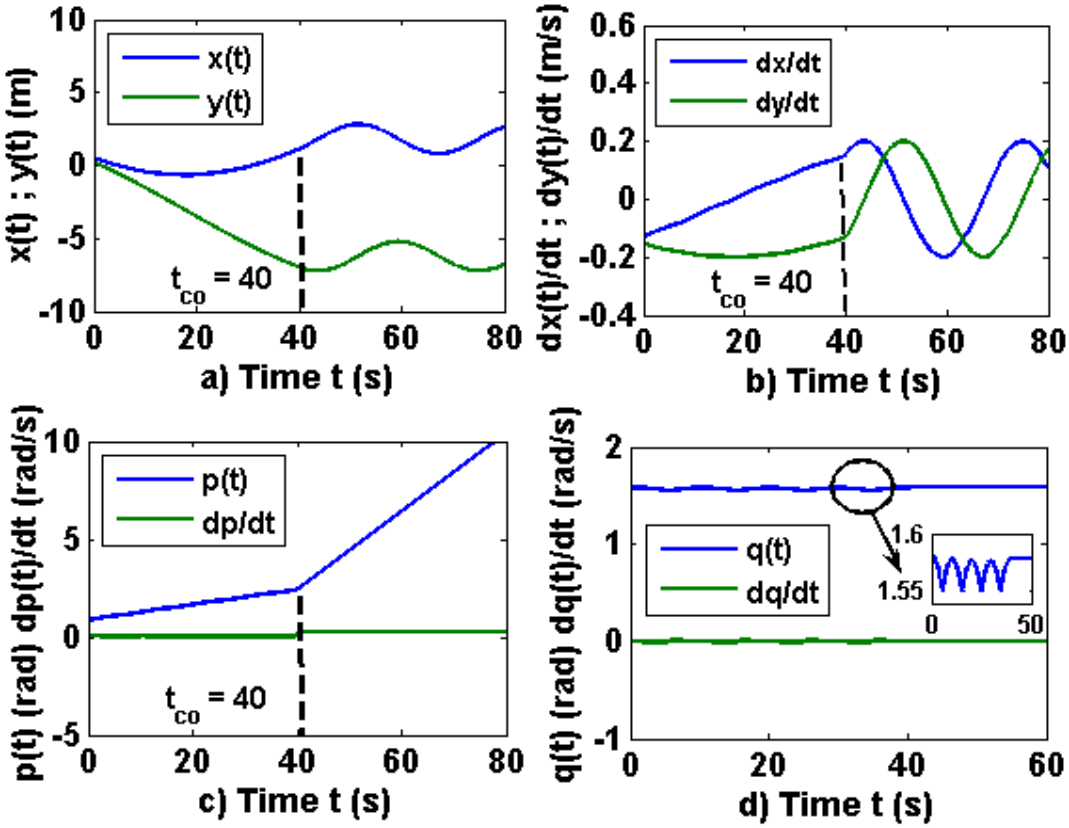
x(t) ; y(t) (m)
x(t)
y(t)
t_co = 40
a) Time t (s)
dx(t)/dt ; dy(t)/dt (m/s)
dx/dt
dy/dt
t_co = 40
b) Time t (s)
p(t) (rad) dp(t)/dt (rad/s)
p(t)
dp/dt
t_co = 40
c) Time t (s)
q(t) (rad) dq(t)/dt (rad/s)
q(t)
dq/dt
1.6
1.55
0
50
d) Time t (s)

Figure 7

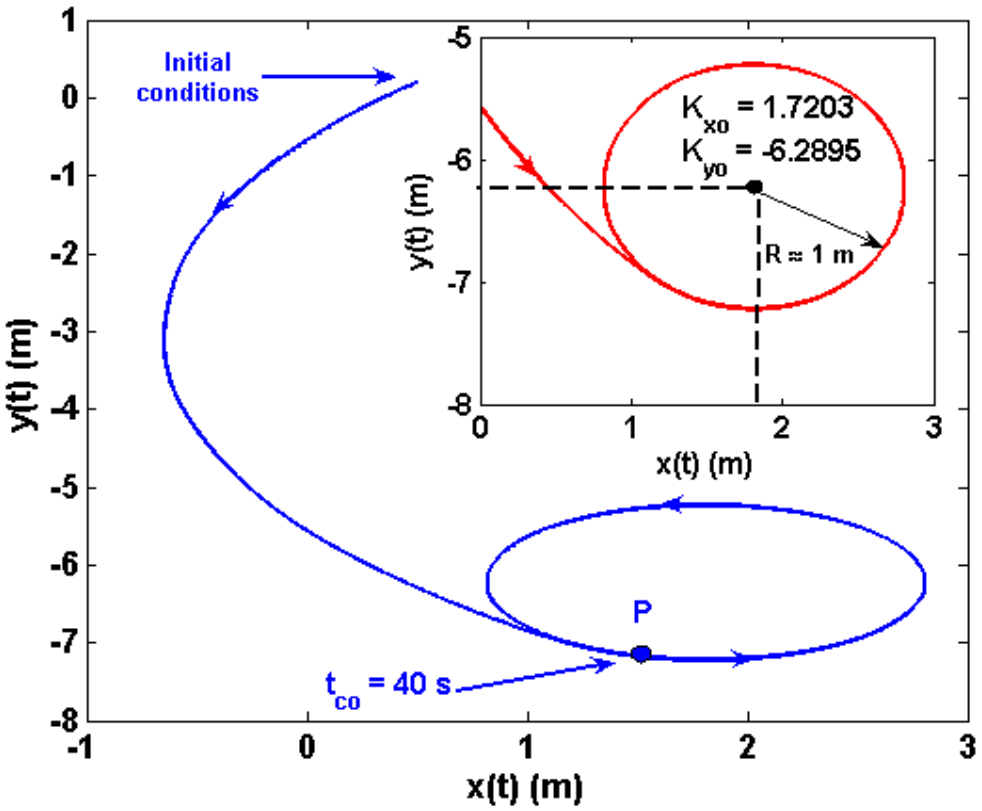

Figure 8

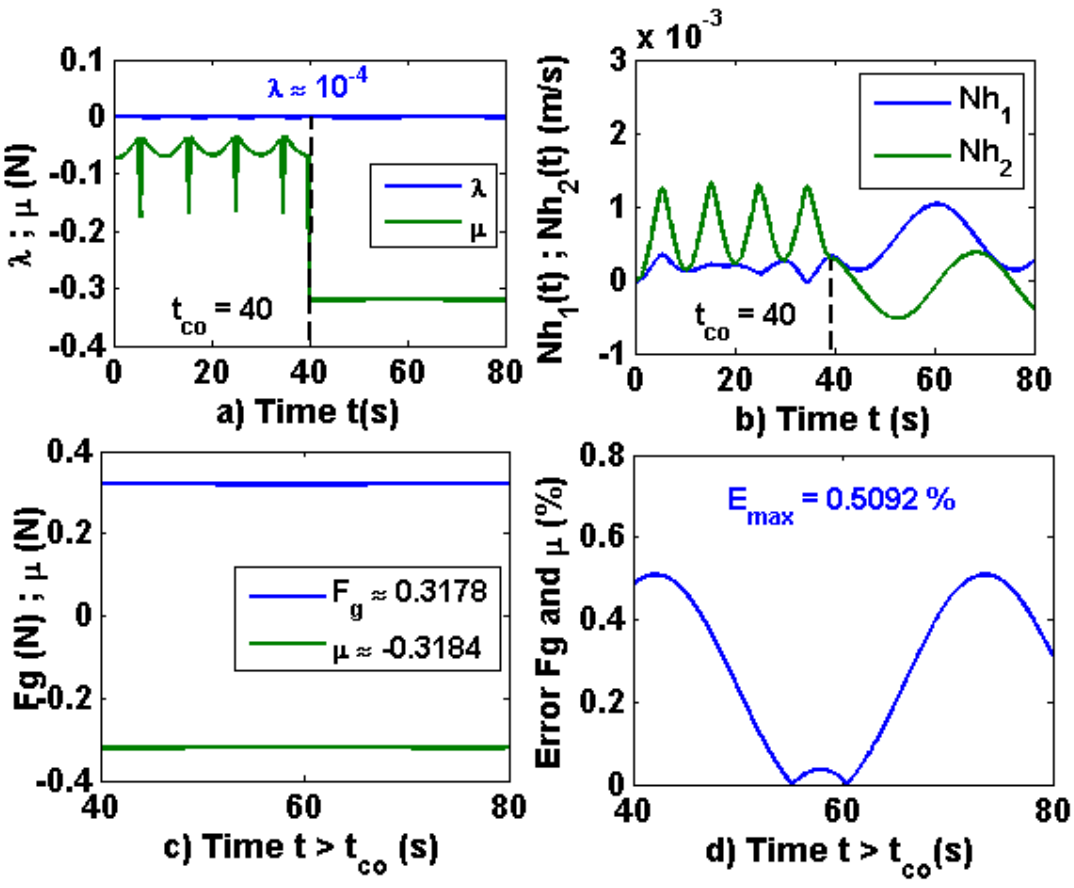
λ ≈ 10^-4
λ
μ
t_co = 40
λ ; μ (N)
a) Time t(s)
x 10^-3
Nh_1
Nh_2
Nh_1(t) ; Nh_2(t) (m/s)
b) Time t (s)
F_g ≈ 0.3178
μ ≈ -0.3184
Fg (N) ; μ (N)
c) Time t > t_co (s)
E_max = 0.5092 %
Error Fg and μ (%)
d) Time t > t_co(s)

Figure 9

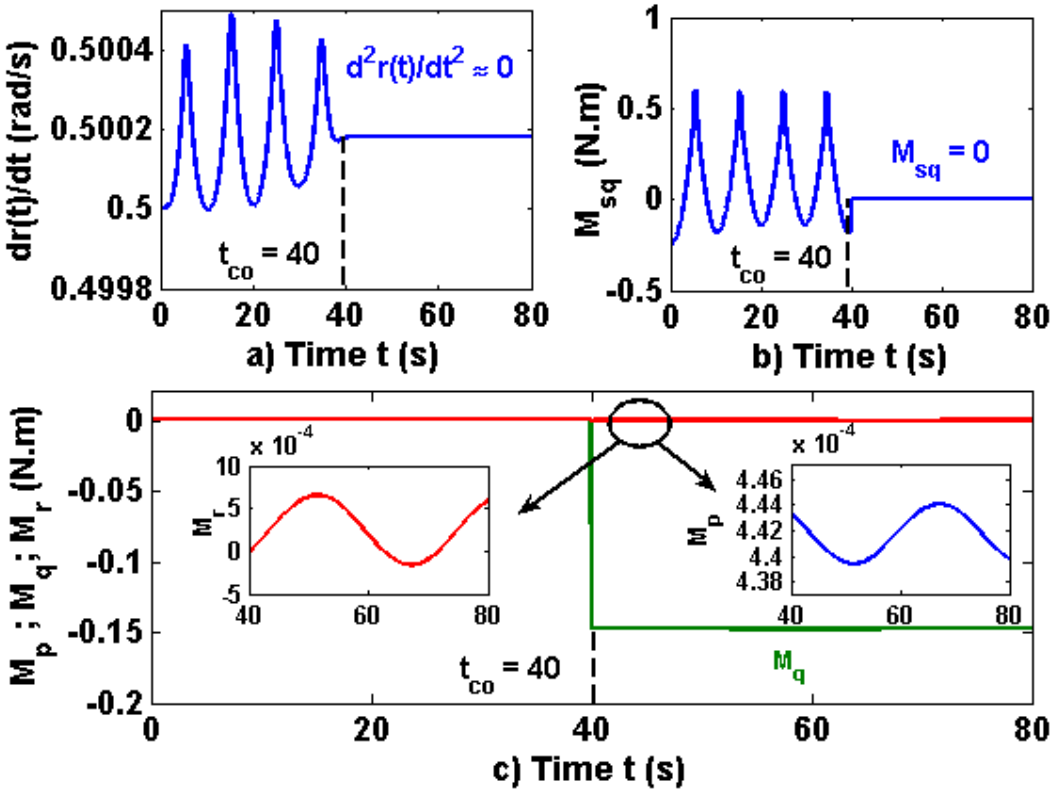
dr(t)/dt (rad/s)
0.5004
0.5002
0.5
0.4998
d²r(t)/dt² ≈ 0
t_co = 40
0
20
40
60
80
a) Time t (s)
M_sq (N.m)
1
0.5
0
-0.5
M_sq = 0
t_co = 40
b) Time t (s)
M_p ; M_q ; M_r (N.m)
0
-0.05
-0.1
-0.15
-0.2
x 10^-4
10
5
0
-5
M_r
x 10^-4
4.46
4.44
4.42
4.4
4.38
M_p
t_co = 40
M_q
c) Time t (s)

Figure 10

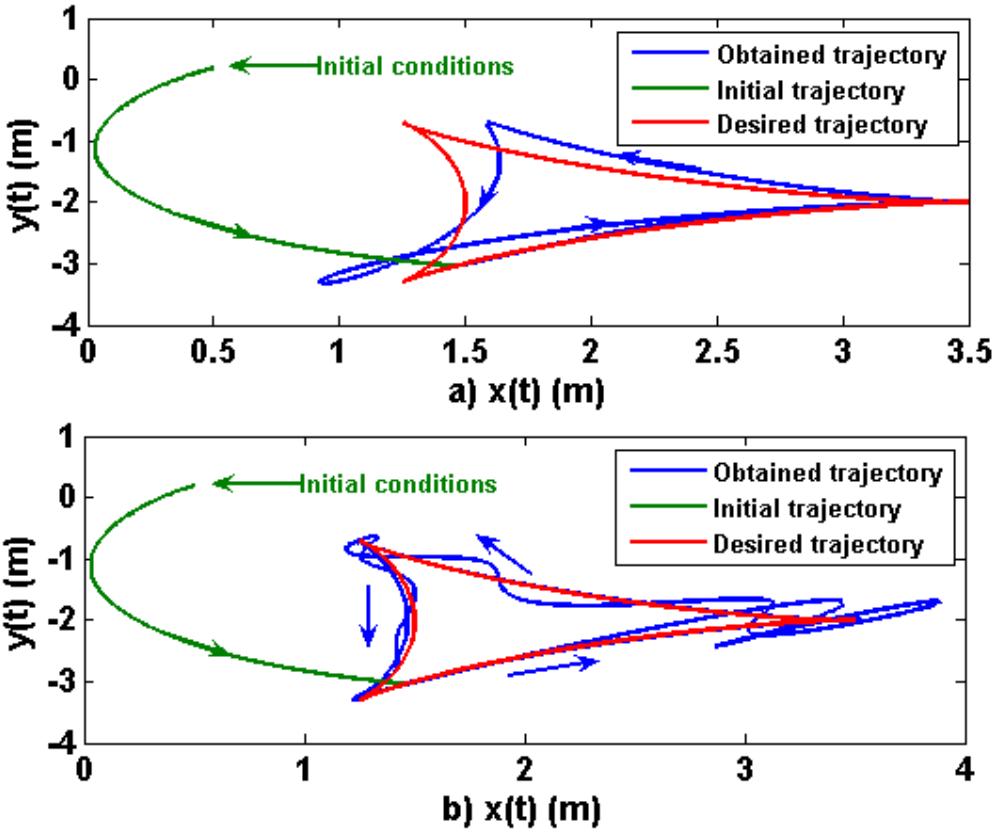
Initial conditions
Obtained trajectory
Initial trajectory
Desired trajectory
y(t) (m)
a) x(t) (m)
Initial conditions
Obtained trajectory
Initial trajectory
Desired trajectory
y(t) (m)
b) x(t) (m)

Figure 11

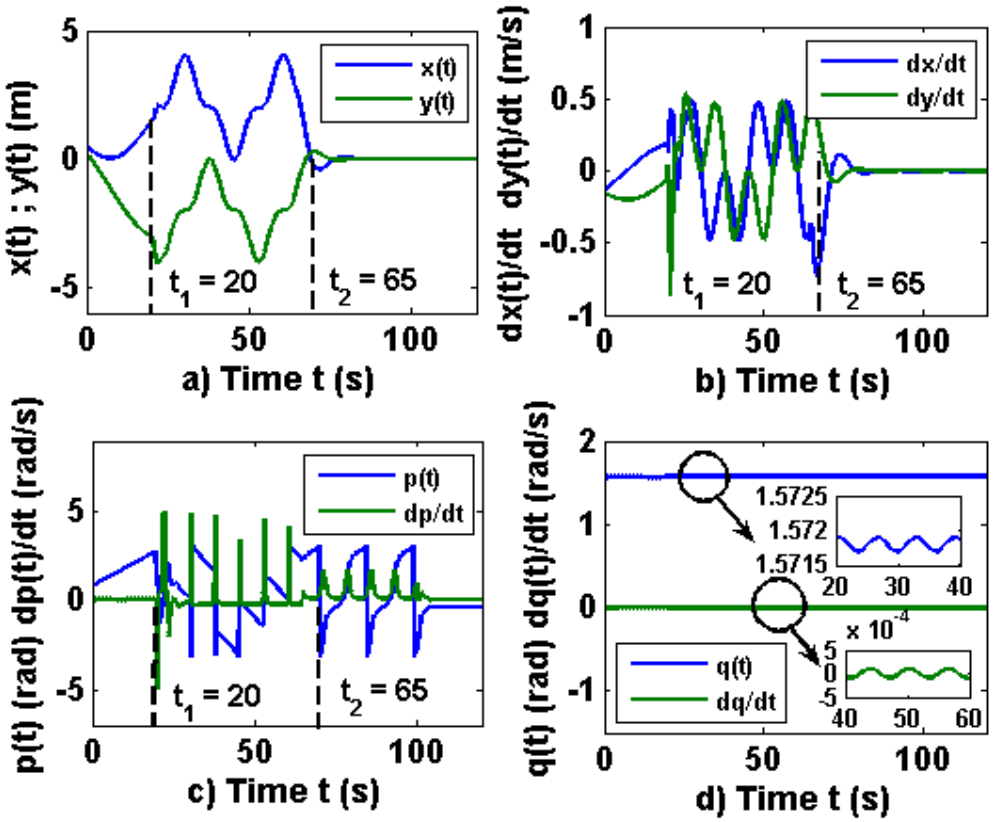
x(t) ; y(t) (m)
x(t)
y(t)
t1 = 20
t2 = 65
a) Time t (s)
dx(t)/dt dy(t)/dt (m/s)
dx/dt
dy/dt
t1 = 20
t2 = 65
b) Time t (s)
p(t) (rad) dp(t)/dt (rad/s)
p(t)
dp/dt
t1 = 20
t2 = 65
c) Time t (s)
q(t) (rad) dq(t)/dt (rad/s)
1.5725
1.572
1.5715
x 10^-4
q(t)
dq/dt
d) Time t (s)

Figure 12

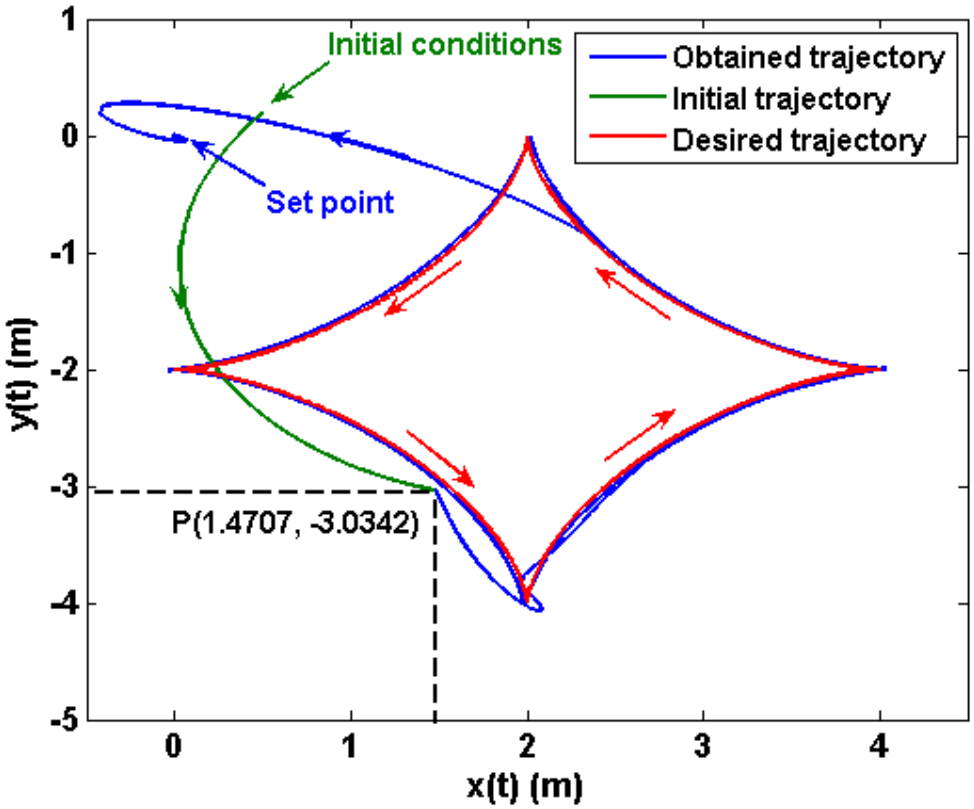
Initial conditions
Obtained trajectory
Initial trajectory
Desired trajectory
Set point
P(1.4707, -3.0342)
y(t) (m)
x(t) (m)
1
0
-1
-2
-3
-4
-5
0
1
2
3
4

Figure 13

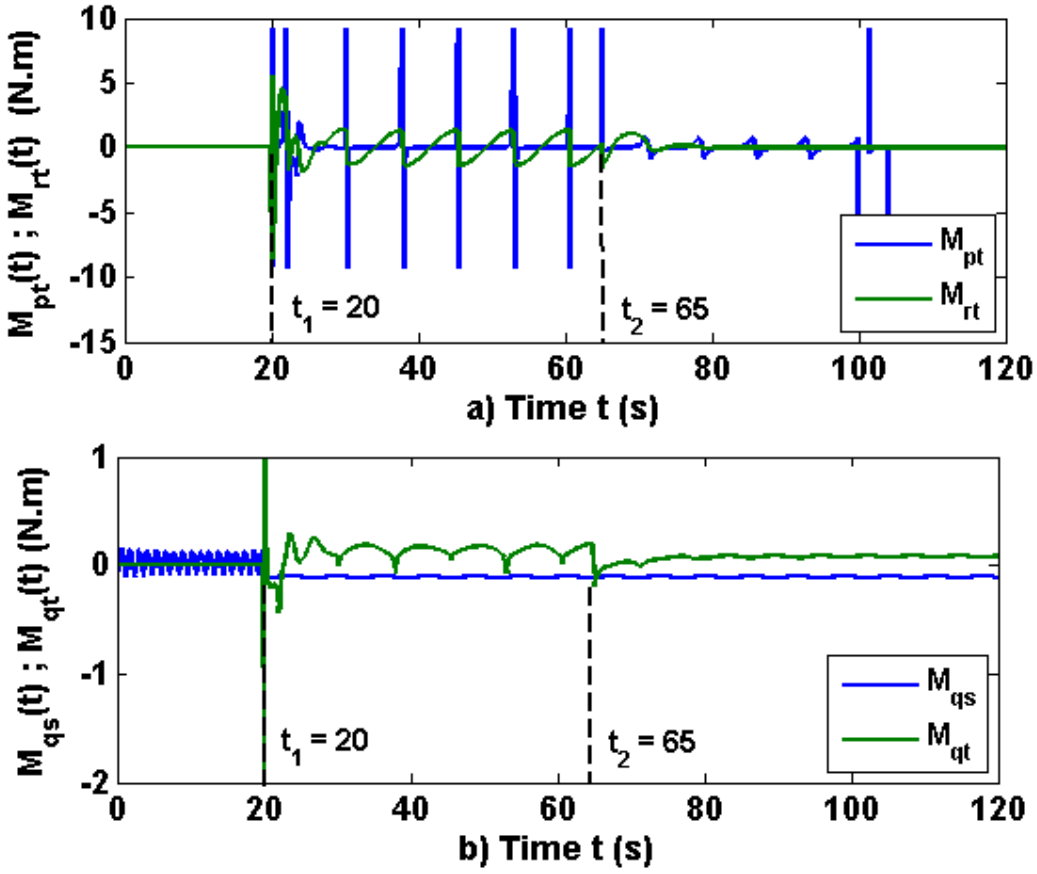
$M_{pt}(t)$; $M_{rt}(t)$ (N.m)
10
5
0
-5
-10
-15
0
20
40
60
80
100
120
t_1 = 20
t_2 = 65
M_{pt}
M_{rt}
a) Time t (s)
$M_{qs}(t)$; $M_{qt}(t)$ (N.m)
1
0
-1
-2
0
20
40
60
80
100
120
t_1 = 20
t_2 = 65
M_{qs}
M_{qt}
b) Time t (s)

Figure 14

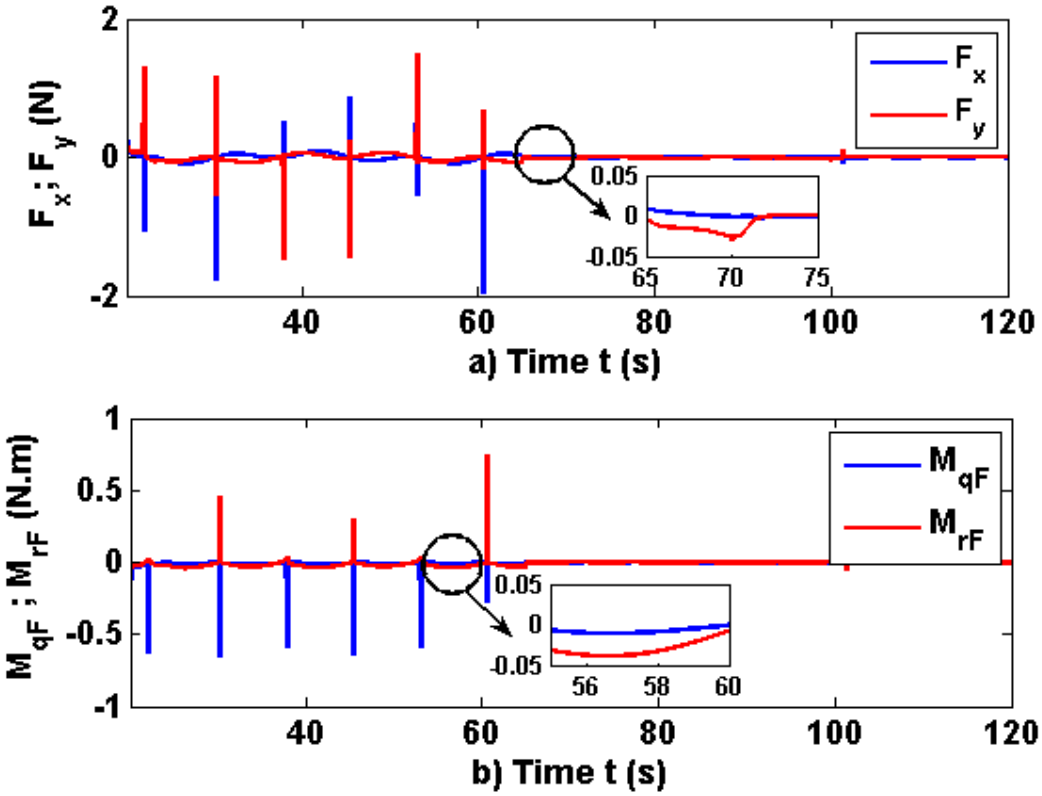

Figure 15

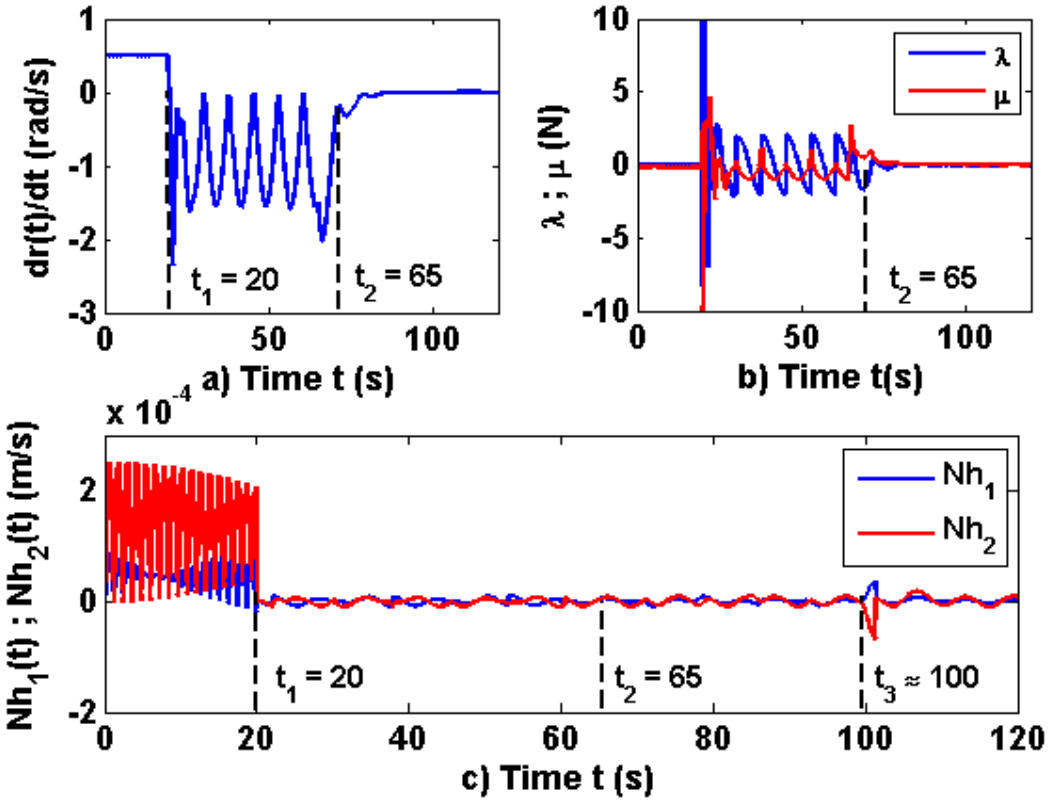
dr(t)/dt (rad/s)
t1 = 20
t2 = 65
a) Time t (s)
λ ; μ (N)
λ
μ
t2 = 65
b) Time t(s)
x 10-4
Nh1(t) ; Nh2(t) (m/s)
Nh1
Nh2
t1 = 20
t2 = 65
t3 ≈ 100
c) Time t (s)

Figure 16

Legend of figures

Figure 1. a) Wheel rolling on a horizontal plane with reaction forces λ and μ. The Euler angles and their derivatives are denoted by *(p,q,r)* and $(\dot{p},\dot{q},\dot{r})$ respectively. The inertial system is OXYZ whereas $G\xi\eta\varsigma$ is the reference system bound to the body. b) Cross section of the wheel that is used to determine the generalized torques. c) Scheme showing an infinitesimal displacement of the contact point C to determine the nonholonomic constraints. The parameter values are a = 0.1 m, b = 0.3 m, M = 5 kg (wheel mass), M_1 = *3* kg (servomechanism mass) and $M_T = M+M_1$ = *8* kg. The equatorial and polar moments of inertia are A_e = 0.2875 kgm^2 and C_p = 0.5250 kgm^2 respectively.

Figure 2. a) Reference systems *'o', 'i', 's'* and *'p_b'* associated to the wheel motion, which are necessary to define a surface element of the wheel with respect to the inertial system OXYZ. b) Basic geometry of the wheel to determine its kinetic energy by integration along its surface.

Figure 3. a) Trajectory of the wheel in the absence of control torques and with a large angular velocity of 10 rad/s. b) The angular velocity of the wheel remains approximately constant. c) Reaction forces at the contact point between the wheel and the supporting plane OXY, being the longitudinal force λ very small. d) The nonholonomic constraints are negligible and thus the condition of rolling without slipping is verified.

Figure 4. a) Effect of a friction torque M_r = -0.3 Nm due to the non ideal contact between the wheel and the supporting plane OXY. For $t = t_2$ the wheel drops and the coordinates *(x,y)* remain constant. b) Velocities associated to the values of *x(t)* and *y(t)* depicted in Fig 4 a). c) Trajectory of the contact point in the OXY plane. d) Precession and angular velocities as functions of the time.

Figure 5. Effect that a friction torque M_r = -0.3 Nm produces on the leaning angle and its velocity. b) Angular velocity of the wheel. For $t < t_1$ the velocity decreases and for $t \geq t_1$ the wheel drops. c) Variation of the reaction forces in the OXY plane against time, where the abrupt change is due to the dropping of the wheel. d) Nonholonomic conditions as functions of the time. As expected, such nonholonomic conditions are not fulfilled while the wheel drops.

Figure 6. Kinetic energy, potential energy, dissipated energy due to the friction torque and total energy of the wheel, all of them plotted against time.

Figure 7. a) Coordinates of the contact point between the wheel and the supporting plane plotted against time. For $t \geq 40$ s the radius of the circular trajectory remains R ≈ 1 m. b) Velocities associated to the trajectory of the contact point shown in a). c) Precession angle and its velocity as functions of the time. d) Leaning angle and its velocity as functions of the time.

Figure 8. Trajectory tracked by the contact point between the wheel and the supporting plane. For t ≥ 40 s the trajectory radius remains R ≈ 1 m.

Figure 9. a) Reaction forces at the contact point between the wheel and the supporting plane. For $t \geq 40$ s the lateral reaction force μ remains approximately constant. b) Nonholonomic conditions against time. c) Dynamical equilibrium between the centrifugal and lateral reaction forces. d) Relative error between the centrifugal and lateral reaction forces as a function of the time.

Figure 10. a) Angular velocity of the wheel plotted against time. For $t \geq 40$ s the angular velocity remains constant. b) Stabilizing torque as a function of the time. c) Control torques within the circular motion of the wheel.

Figure 11. Trajectories obtained for different integral actions of the PID controller. The desired trajectory is an astroid with three cusp points assuming: a) $\tau_{ix} = \tau_{iy} = 10^{10}$ s (negligible integral action) and b) $\tau_{ix} = \tau_{iy} = 0.3$ s.

Figure 12. a) Coordinates of the contact point between the wheel and the supporting plane to track an astroid curve with four cusp points and with final position at the set point (0,0). b) Velocities corresponding to coordinates shown in a). c) Precession angle and its corresponding velocity versus time. d) Leaning angle and its corresponding velocity versus time. The results have been obtained with a simulation time of 120 s, a simulation step of 0.005 s and the initial conditions given by Eq (66).

Figure 13. Initial trajectory only with the stabilizing torque given by Eq (55). Desired trajectory to reach the astroid with four cusp points. Tracked trajectory to reach the set point (0,0).

Figure 14. a) Control torques around the precession and pealing angle to reach the desired trajectory for $20 < t \leq 65$ s. b) Stabilizing torque given by Eq (55) and leaning torque deduced from the second equation of (64) assuming $A_q = 10^{-4}$ rad and $\omega_q = 1$ rad/s.

Figure 15. a) Terms F_x and F_y deduced from Eqs (74), which are plotted for $20 < t \leq 65$ s (the astroid curve is tracked) and for $t > 65$ s (the set point (0,0) is reached). b) Torques M_{qF} and M_{rF} (which give raise to F_x and F_y) around the leaning angle and the precession angle deduced from Eqs (82), which are plotted for $20 < t \leq 65$ s (the astroid curve is tracked) and for $t > 65$ s (the set point (0,0) is reached).

Figure 16. a) Angular velocity of the wheel as a function of the time. The astroid curve is tracked for $20 < t \leq 65$ s whereas the set point is reached for $t > 65$ s. b) Reaction forces at the contact point between the wheel and the supporting plane plotted against time, which are approximately zero when the set point is reached (for $t > 65$ s). c) Nonholonomic constraints plotted against time. This conditions are very small for $20 < t \leq 65$ s when the astroid curve is tracked, whereas they are not exactly equal to zero for $t > 65$ s due to the application of the stabilization torque.